Graduate School Form 30
Updated 1/15/2015

PURDUE UNIVERSITY
GRADUATE SCHOOL
Thesis/Dissertation Acceptance

This is to certify that the thesis/dissertation prepared

By RANI VIJAYA PENUMAKA

Entitled

SYNTHESIS OF LITHIUM MANGANESE PHOSPHATE BY CONTROLLED SOL-GEL METHOD AND DESIGN OF ALL SOLID STATE LITHIUM ION BATTERIES

For the degree of Master of Science in Mechanical Engineering

Is approved by the final examining committee:

LIKUN ZHU
Chair

JING ZHANG
Co-chair

YONGZHU FU
Co-chair

To the best of my knowledge and as understood by the student in the Thesis/Dissertation Agreement, Publication Delay, and Certification Disclaimer (Graduate School Form 32), this thesis/dissertation adheres to the provisions of Purdue University's "Policy of Integrity in Research" and the use of copyright material.

Approved by Major Professor(s): LIKUN ZHU

Approved by: JIE CHEN 4/27/2015
Head of the Departmental Graduate Program Date

SYNTHESIS OF LITHIUM MANGANESE PHOSPHATE BY CONTROLLED SOL-GEL METHOD AND DESIGN OF ALL SOLID STATE LITHIUM ION BATTERIES

A Thesis

Submitted to the Faculty

of

Purdue University

by

Rani Vijaya Penumaka

In Partial Fulfillment of the

Requirements for the Degree

of

Master of Science in Mechanical Engineering

May 2015

Purdue University

Indianapolis, Indiana

ACKNOWLEDGEMENTS

"I will give you thanks in the great congregation: I will praise you among much people - Psalms 35:18."

I would like to express my greatest gratitude to my advisor, Dr. Likun Zhu, for his supervision, guidance and financial assistance throughout my study in the Master's degree program. Dr. Zhu was always like a friend to me and shared his knowledge and research experience, for which I am always obliged. More importantly, I will forever be thankful and indebted to my co-advisors, Dr. Youngsik Kim and Dr Jae-Kwang Kim. Although Dr. Youngsik Kim was my advisor for few months before he left to South Korea, I am very thankful for his help in familiarizing me with the solid-state project and giving me deep knowledge in the lithium ion batteries. Also, my sincere acknowledgements are given to Dr Jae-Kwang Kim for supervising me in all the $LiMnPO_4$ projects' from South Korea. He was highly patient during all my thesis work and with his timely advice and guidance, helped me a lot in finishing my thesis.

Finally, I would like to thank my thesis committee members Dr. Yongzhu Fu and Dr. Jing Zhang for their time and participation in my thesis defense. Their advice and comments have further enriched the quality of this thesis.

In addition, I extend thanks to Ms. Valerie Lim Diemer for assisting me with formatting my thesis. And I would also like stretch out my heart full thanks to my family and friends, who inspired me in this journey. This work is supported by National Science Foundation under Grant number 1335850.

TABLE OF CONTENTS

Page

LIST OF TABLES

LIST OF FIGURES

Figure Page

Figure Page

ABSTRACT

Penumaka, Rani Vijaya. M.S.M.E., Purdue University, May 2015. Synthesis of Lithium Manganese Phosphate by Controlled Sol-Gel Method and Design of All Solid State Lithium Ion Batteries. Major Professor: Likun Zhu.

Due to the drastic increase in the cost of fossil fuels and other environmental issues, the demand for energy and its storage has risen globally. Rather than being dependent on intermittent energy sources like wind and solar energy, focus has been on alternative energy sources. To eliminate the need for fossil fuels, advances are being made to provide energy for hybrid electric vehicles (HEV), plug-in hybrid vehicles (PHEV) and pure electric vehicles (EV) thus providing scope for much greener environment. Hence, focus has been on development in lithium ion batteries to provide with materials that have high energy density and voltage.

Ortho olivine lithium transitional metals are known to be abundant and inexpensive; these compounds are less noxious than other cathode materials. Advancement in research is being done in finding iron and manganese compounds as cathode materials for advanced technologies. However, Lithium manganese phosphates are known to suffer with poor electrochemical performances due the manganese dissolution in the organic liquid electrolyte due to Jahn-Teller Lattice distortion. This problem was tried to endorse in this thesis. In the second chapter by synthesizing nano sized cathode particles with good electronic conductivity, good performance was achieved.

In the third chapter additive olivine cathode was synthesized my modified sol gel process. A wt. % of TMSP was added as an additive in the organic liquid electrolyte. By comparing the properties between the two kinds of electrolytes it was observed that by the addition of the additive in the organic electrolyte good electrochemical properties could be achieved hindering the Mn dissolution in the electrolyte.

In the final chapter, a composite solid electrolyte was fabricated by using NASICON-type glass ceramic of Lithium aluminum titanium phosphate (LATP) with organic binder of Polyethylene oxide. The flexible solid electrolyte exhibited good ionic conductivity. An all solid state cell was fabricated using the composite solid electrolyte using $LiMn_2O_4$ as the symmetric electrodes. At different pressures, the performance of the solid state cell was studied.

1 INTRODUCTION

1.1 Overview of Lithium Ion Batteries

Due to the drastic increase in the cost of fossil fuels and other environmental issues, the demand for energy and its storage has risen globally. To eliminate the need for fossil fuels, advances are being made to provide energy storage systems for hybrid electric vehicles (HEV), plug-in hybrid vehicles (PHEV) and pure electric vehicles (EV) thus providing scope for much greener environment.

Currently a lot of effort is put on achieving high energy density batteries, which are dependent on the basic cell chemistry, that are reflected by the cell's potential and capacity. The cost and safety are also very important for EV applications. With intrinsic properties like high energy density, high efficiency, superior rate capability, and long cycling life, lithium ion battery (LIB) stands as a forerunner and market leader in the application of portable electronics. Since their commercialization in 1991, the size ranged from few microns to a large-scale battery that is capable of providing energy for portable electronics and EVs.

The energy density per unit volume (Wh/1) and per unit weight (Wh/kg) of various secondary batteries are shown above. As seen from the Figure 1.1, nickel metal hydride and LIBs have higher volume energy density, but LIB has 1.5 times more energy density when compared to nickel hydride batteries. The nominal voltage of LIBs is higher when compared to the rest of the batteries.

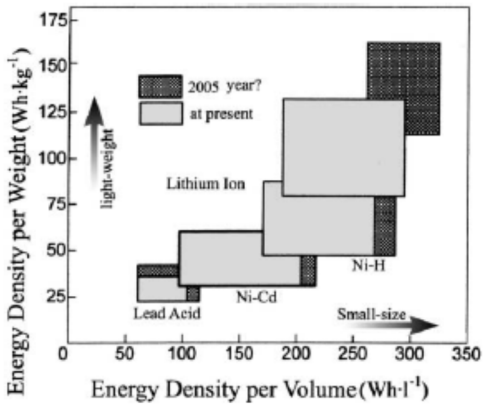

Figure 1.1 Energy density of secondary batteries [1]

1.1.1 Concept of Batteries

A device that converts chemical energy stored in the active materials to electrical energy through a redox (oxidation-reduction) reaction is referred as "battery". One electrode gives up the electrons and gets oxidized, while the other accepts the electrons and gets reduced. Electrolyte, typically an ionic conductor, acts as a medium for transfer of charge. Batteries are capable of delivering higher efficiency as they are not limited by Carnot efficiency.

1.1.2 Operation of a Battery

1.1.2.1 Discharge

When an external load is applied, anode gets oxidized and electrons flow to the cathode where they are accepted and due to which cathode gets reduced. To counter the flow of electrons, ions (cations and anions) flow through the electrolyte to the anode and cathode as shown in Figure 1.2.

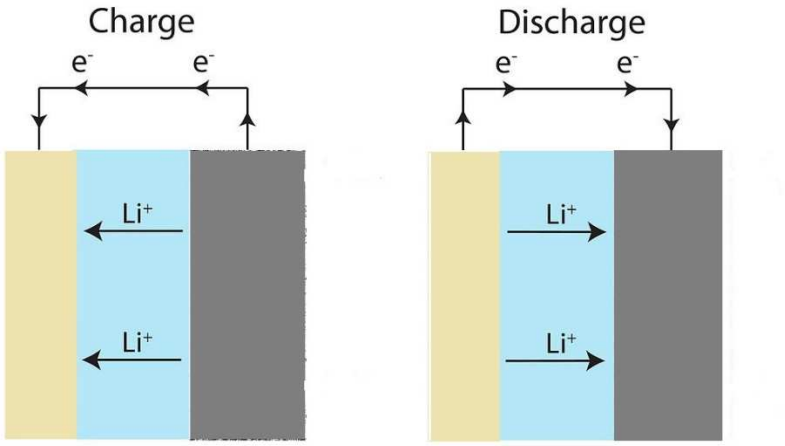

Figure 1.2 Charge/discharge schematic of Li ion battery

1.1.2.2 Charge

During this process, the flow of current is reversed as shown in Figure 1.2. At the cathode, oxidation takes place and reduction takes place at the anode electrode.

1.1.3 Free Energy

During the conversion of the chemical energy to electrical energy, the maximum energy that can be delivered by the battery depends on the change in free energy ΔG of the electrochemical couple. Hence the change in free energy is,

$$\Delta G = -nFE^{\circ}$$

Where F = Faraday's constant (~96,500 C)

n = Number of electrons involved in the reaction

E° = Standard potential

1.1.4 Standard Potential

The theoretical voltage of the cell is determined by the reactants of the cell. It can be calculated from the standard electric potentials of the reacting species.

Anode (Oxidation Potential) + Cathode (Reduction Potential) = Standard Cell Potential.

Not all theoretically stored energy is converted to electrical energy because of the losses due to polarization occurring when a load current passes through the electrodes. These losses occur due to

(1) Activation Polarization
(2) Concentration Polarization
(3) Ohmic Polarization

Thus, the cell voltage E can be calculated as

$$E = E^{\circ} - [(\eta_{ct})_a + (\eta_c)_a] - [(\eta_{ct})_c + (\eta_c)_c] - iR_i = iR$$

Where E°= Open circuit voltage

$(\eta_{ct})_a$, $(\eta_{ct})_c$ = Activation Polarization

$(\eta_c)_a$, $(\eta_c)_a$ = Concentration Polarization

i = Load Current

R_i = Internal resistance of cell

1.1.5 Capacity

Capacity depends on the amount of the active materials in the cell. It is defined as the total quantity of charges involved in the electrochemical reaction and its unit is coulombs or ampere-hours.

1.2 Working Principle of Lithium Ion Batteries

These batteries are designed in accordance with the reversible capacity of the carbon materials used as anode, and any metal oxide material as cathode in electrolyte wherein lithium does not exist in metallic state during either charge or discharge process hence are termed as “lithium ion batteries”.

Lithium ion batteries employ lithium intercalation compounds as the cathode and anode materials. Lithium ion rechargeable battery is often referred as rocking chair or swing battery, as Lithium ions move in a two-way motion between cathode and anode for charge/discharge phenomenon. In this type, instead of using Lithium metal, an intercalated lithium compound is used as an electrode material. The cathode material is typically a metal oxide such as $LiCoO_2$ or $LiMn_2O_4$ on a current collector such as Aluminum. The anode electrode is typically a graphitic carbon on a copper current collector. During the charge and discharge processes, the lithium ions get inserted and extracted between the interstitial space lying in the atomic layers of the cathode and anode materials.

1.2.1 Design Criteria

In a Lithium ion battery, the open circuit potential (V_{OC}) is given by the difference of the chemical potential of the cathode (μ_c) and the anode (μ_a), given by,

$$V_{OC} = (\mu_c - \mu_a)/F$$

Where, F = Faraday constant (96485 C/mol)

The energy involved in the electron and lithium ion transfer determines the cell potential. In turn, the redox potential of the ion present in the cathode and anode determines the energy involved in electron transfer. While the coordination geometry and crystal structure of the active materials involved determines the energy involved in lithium transfer [2]. Thermodynamics requires that the redox energies of the cathode (μ_c) and anode (μ_a)

lie in the stability window of the electrolyte, as shown in the Figure 1.3. The stability window of the electrolyte depends on the energy gap (E_g) that is the difference between the lower unoccupied molecular orbital (LUMO) and the highest occupied molecular orbital (HUMO) of the electrolyte.

Hence, for the design of a battery, the anode should have its μ_a below the LUMO and the cathode should have its μ_c above HUMO of the electrolyte. Sometimes, a suitable solid electrolyte interface (SEI) is formed to prevent reduction/oxidation between the active materials and electrolyte. Thus, the cell voltage limitations according the electrochemical stability window requires,

$$V_{OC} = (\mu_C - \mu_A)/F \leq E_g$$

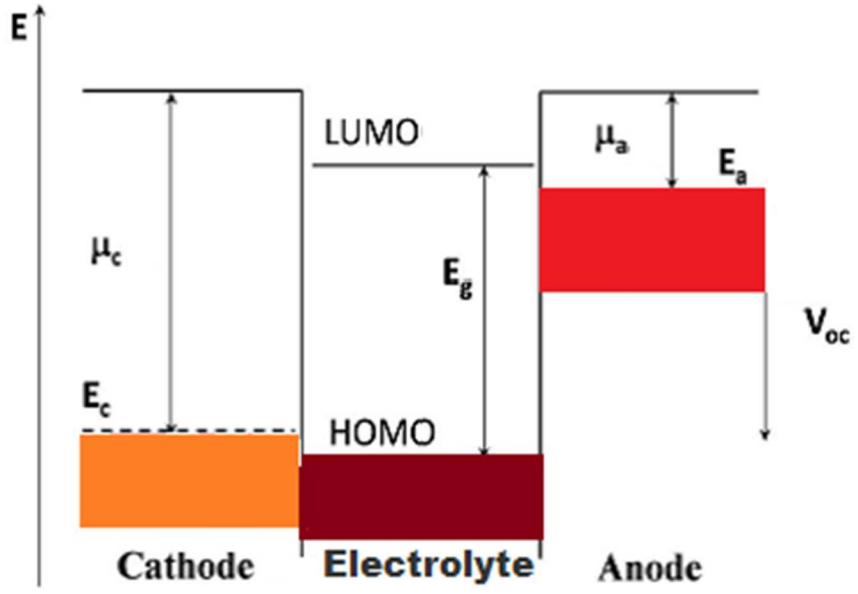

Figure 1.3 Stability window of the electrolyte

1.2.2 Positive Electrode Material

The major requirements of cathode materials are

- Should reversibly incorporate lithium without structural changes
- Incorporate large amounts of Lithium
- Good free energy of reaction with lithium
- High Lithium ion diffusivity
- Good electronic conductivity
- Non soluble in electrolyte
- Ease of synthesis
- Cheap

Mostly all the cathodes currently are intercalated materials, typically lithium transition metal dichalcogenides. These materials contain insertion sites that are occupied by lithium ions. During this process, the transition metal ion reduces by accepting an electron.

By demonstrating electrochemical activity in layered $LiTiS_2$ in the 1970s, Whittingham[3] was the first to introduce commercial intercalation cathode. Later in 1980s, layered $LiCoO_2$ that currently dominates in today's technology was discovered be Mizushima et al [4]

The conventional cathodes are typically layered compounds $LiMO_2$ (M = Co,Ni,Mn, etc.), spinel compounds LiM_2O_4 (M = Mn, Fe, etc.), and olivine compounds $LiMPO_4$ (M = Fe, Co, Mn, etc.).

Table 1 gives some cathode materials of rechargeable batteries and their properties [5]

Table 1.1 Cathode materials and their properties [5]

	$LiCoO_2$	$LiNiO_2$	$LiMn_2O_4$	$Li[Ni_{1/3}Co_{1/3}Mn_{1/3}]O_2$	$Li[Ni_{1/2}Mn_{1/2}]O_2$	$LiFePO_4$
Theoretical capacity	274 mAh/g	275 mAh/g	148 mAh/g	285 mAh/g	285 mAh/g	170 mAh/g
Available Capacity	145 mAh/g	185 mAh/g	120 mAh/g	170 mAh/g	170 mAh/g	150 mAh/g
Voltage	3.7 V	3.6 V	3.8 V	3.7 V	3.7 V	3.45V
Advantage	High conductivity Easy synthesis	- High capacity - Stability of electrolyte	- Low price - Non-toxic	- High capacity - Low price - Good thermal stability	- High capacity - Low price - Good thermal stability	- Low Price - Environmental friendly
Disadvantage	- High cost - Toxic	- Difficult synthesis and fabrication of thin film - Thermal instability	- Low capacity - Capacity fading @ High Temp	- Low tap density compared to $LiCoO_2$	Low conductivity ($<10^{-8}$ S/cm)	Low Conductivity ($<10^{-9}$ S/cm)

1.2.3 Negative Electrode Material

Early 1980s and 1970s focuses were on using Lithium metal as anode, but due to safety issues lithium intercalation into carbon as the negative electrode are used instead. Unlike lithium metal that changes its surface morphology during cycling, carbon electrodes offer better stability.

The structure, precipitation temperature of carbon is highly significant on its electrochemical properties, even on the lithium intercalation capacity and potential [6]. Among all types of carbon, graphite has optimal properties and hence is widely used in commercial LIBs. The theoretical specific capacity of carbon (LiC_6) is 372 mAh/g [7].

1.2.4 Electrolyte

Electrolyte is a medium that provides transfer of ions between the cathode and anode. Together with high ionic conductivity, they should be compatible with electrodes.

Electrolytes are basically characterized into four types: liquid electrolytes, gel electrolytes, polymer electrolytes and ceramic electrolytes.

Liquid electrolytes contain lithium salt in organic solvents, typically carbonates. A polymer electrolyte is formed by adding a salt in a high molecular weight polymer, where an ion conducting phase is formed. A gel electrolyte contains both salt and solvent are dissolved in a high molecular weight polymer. The ceramic electrolytes are inorganic, solid-state materials that are ion conductive.

The popular lithium salts are $LiPF_6$, $LiBF_4$, and $LiAsF_6$. $LiPF_6$ is widely used among them as it offers high conductivity (>10^{-3} S/cm), high lithium transference number (~0.35) and acceptable safety [8]. Electrolytes are mostly formulated using carbonates such as ethylene carbonate (EC), propylene carbonate (PC), dimethyl carbonate (DMC), as they are aprotic, polar and able to dissolve Lithium ions to high concentration.[9] Typically multiple solvents are used as they provide better performance, high conductivity and broad temperature range.

Special focus will be given in the later sections about the solid state electrolytes used in lithium ion batteries.

1.2.5 Separator

Separator is a porous film between the two electrodes to prevent short circuit. The separator itself does not take part in any reaction inside the lithium ion battery but allows only ionic transport preventing electron transport. It should be chemically and mechanically stable along with good porosity to absorb the liquid electrolyte inside the lithium ion battery. However, the separator should be as thin as possible to avoid any space wastage, thereby increasing the battery energy density. Most common separators for secondary batteries are polyethylene (PE) and polypropylene (PP). The separators also

prevent the cell from overheating. However, they cannot function above their melting point. Melting point of PP is 170˚C [10, 11]

1.2.6 Current Collector

The current collectors used for electrodes in LIB also affect the anodic stability of the electrolyte solutions. Most of the common metals in the potential range up to 5V vs Li dissolve in aprotic electrolyte solutions. Inert metals as Pt, Au cannot be considered due to their cost. For current LIBs, Cu is used as anode current collector and Al is used as cathode current collector [12].

1.3 Olivine Type Lithium Transition Metal Phosphates as Cathode

1.3.1 Overview

Advancement in research is being done in finding iron and manganese compounds as cathode materials. These compounds are abundant, inexpensive, and less noxious than other cathode materials. The significant work was done by Padhi *et al* [13] in 1997, with the discovery of the cathode materials belonging to this system. It has displayed a high potential for the Fe^{2+}/Fe^{3+} redox couple (3.5V) vs Li with a high theoretical capacity of 170mAh/g, since the compound is mineral triphylite it is considered as environment friendly.

To raise the potential of $LiFePO_4$, Fe is replaced by Co or Mn to form $LiCoPO_4$ 4.8V [14, 15, 16] and $LiMnPO_4$ 4.1V [17, 18] respectively. The performance of $LiCoPO_4$ is poor, because of the poor stability of the delithiated cobalt phase ($CoPO_4$) [19].

Hence, the focus was shifted towards $LiMnPO_4$, though it suffers from very low electronic conductivity. It offers various advantages such as a flat voltage discharge profile at 4.1V vs Li/Li^+ [20, 21], low cost, as well as safety features [22, 23]. More importantly

when compared to other polyanion type systems the electrochemical window of this compound falls in the stability window of conventional electrolytes [24]. Different approaches are studied since then to improve the performance of $LiMnPO_4$.

1.3.2 Electronic Structure:

For understanding the electronic structure of $LiMnPO_4$, the Total Density of States (DOS) is shown in the Figure 1.4. The localized 3d states of Mn are the narrow bands in the vicinity of Fermi level [25].

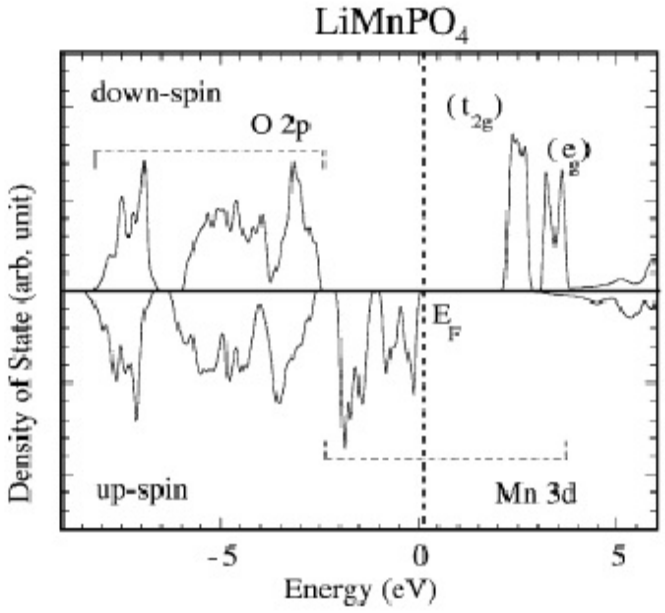

Figure 1.4 Electronic structure of $LiMnPO_4$ [26]

The DOS clearly confirms through the high spin configuration that $LiMnPO_4$ is an insulator with ca. 2eV [26] spin exchange band gap, which explains for the low electrochemical activity of $LiMnPO_4$. From the studies on several first principles electronic structure [27-30] of $LiMnPO_4$ the basic reason for high electrochemical potential of $LiMnPO_4$ can be attributed.

1.3.3 Crystal Structure

The crystal structure of $LiMnPO_4$ is made up of distorted MnO_6 octahedra. The MnO_6 octahedra corners are shared among themselves to form MnO_4 layers parallel to the bc-plane (Figure 1.5)[31]. All the MnO_4 layers are stacked in the a-direction such that the P atoms are at the tetrahedral sites in between the MnO_4 layers to form PO_4 units, while the octahedra sites are occupied by Li atoms as shown in (Figure 1.6)[31]. Layers of MnO_6 octahedra are corner-shared in the bc plane and linear chains of LiO6 octahedra are edge-shared in a direction parallel to the b-axis. The chains are bridged by edge and corner shared phosphate tetrahedral sites, creating a stable 3D structure. $LiMnPO_4$ crystallizes in space group *Pnma*.[32]

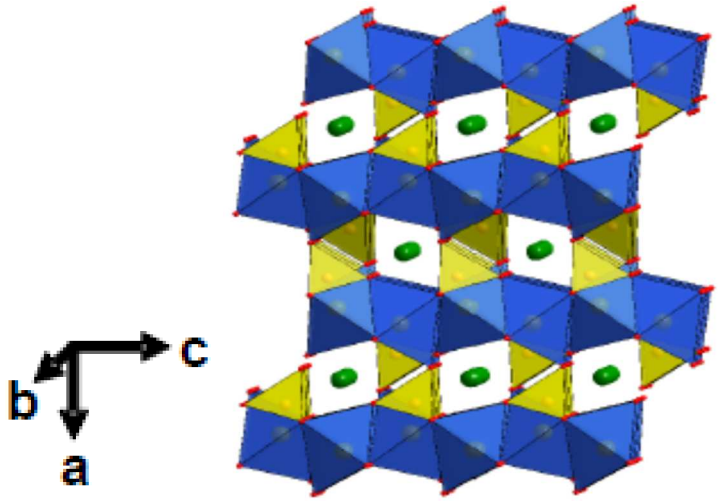

Figure 1.5 Representation of $LiMnPO_4$ along the b-axis [31]

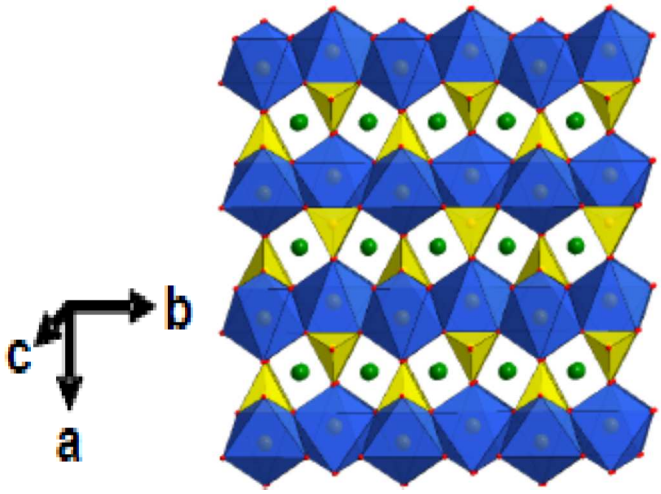

Figure 1.6 Representation of $LiMnPO_4$ along the c-axis [31]

1.3.4 Overview of $LiMnPO_4$ Synthesis Routes

Researchers have focused on realizing the full capability of $LiMnPO_4$ in its native form. This difficulty in utilizing the full performance of $LiMnPO_4$ was proposed due to the following properties:

(1) Low intrinsic electronic conductivity

(2) Jahn-Teller lattice distortion of Mn^{3+} ions

(3) Surface energy barrier for Li diffusion

(4) Metastable nature of the delithiated phase

As $LiMnPO_4$ is more insulating when compared to $LiFePO_4$, several approaches were proposed in the literature to improve the electrochemical kinetics of $LiMnPO_4$. One approach was to combine the particle size reduction with carbon coating. Carbon coating is necessary for $LiMnPO_4$. Fe present in the $LiFePO_4$ offers good catalyst activity to ease the coating process. However, this is lost in the case of $LiMnPO_4$. To be able to achieve the above aim, numerous soft chemical methods were investigated to prepare $LiMnPO_4$ /C. It was found that the performance capability of this cathode material was dependent on nano particle size, which could be achieved by the synthesis route. Since then different

approaches in synthesizing the polyanion framework $LiMnPO_4$ have been focused in the past several years.

Techniques such as solid-state reaction in molten hydrocarbons, polyol route, and spray pyrolysis along with ball milling were studied. Among all, Choi et al. was successfully able to achieve theoretical capacity (~170 mAh/g) at very low C-rate (C/50). He prepared nano-sized rods of 50 nm along the preferred orientation [010]. However, at higher C-rates, the performance was poor [33]. It has been reported that the conductive carbon coating of 20-30 wt% on $LiMnPO_4$ would enable to reach capacities of 130-140 mAh/g [34]. For commercial applications, the carbon wt.% is limited due to the requirement of high energy density. In order to get a conductive carbon coating, calcination temperatures as high as 650°C need to be applied. However, as the calcination temperature increases higher than 650°C, the material rapidly degrades and heterogeneous carbon layer is formed.

Further research in achieving the full potential of $LiMnPO_4$ showed that the calcination temperature of 650°C can be used without degrading the $LiMnPO_4$, only if the particle size was in nanometers [35]. Thus, the researchers started to synthesize the cathode material in nano-size to enhance its properties. Addition of carbon along with precursors was first introduced by Ravet et al [36]. Carbon addition in the initial stages not only prevents particle agglomeration but also helps in deterrence of oxidation.

Li et al [36] synthesized $LiMnPO_4$ /C using a solid state reaction by adding carbon black along with precursors. It was observed that the electrochemical performance was highly dependent on the calcination temperature. At 550°C, highest discharge capacity was obtained. A flat plateau at 4.1V vs Li was obtained during the reversible extraction-insertion of lithium from $LiMnPO_4$. The authors concluded that the limiting factor of $LiMnPO_4$ was mainly due to the low ionic and/or electronic conductivity rather than the slow charge-transfer kinetics.

Using precipitation synthesis route, Delacourt et al. synthesized ~ 100 nm-sized particles of $LiMnPO_4$, which resulted in a reversible capacity of 70 mAh/g at 0.05 C [37].

Kwon et al. used sol-gel technique along with dry ball milling to prepare $LiMnPO_4$/C composite of 130 nm-sized particles, which delivered a reversible capacity of 134 mAh/g at 0.1 C. It was noticed that as the calcination temperature was increased, the Mn^{2+} disorder on the Li^+ sites was reduced. The authors observed that as the C- rate was increased, smaller sized particles were favored [38].

Wang et al. reported that a reversible capacity of 141 mAh/g at 0.1 C rate using trickle mode conditions could be obtained by synthesizing 30 nm thick platelet morphology of $LiMnPO_4$ [39].

Regardless of the preparation approach, most authors used post-synthesis ball milling technique to prepare nano sized $LiMnPO_4$ /C powders. Amongst all the synthesis routes, sol-gel, hydrothermal, and co-precipitation routes were successful.

1.4 Solid State Li Ion Battery

1.4.1 Overview

Considerable focus was put in the research and development in finding alternatives to the commercial liquid electrolyte batteries, in search of stable, safe and high performing lithium ion batteries. To replace the conventional organic electrolyte materials, polymer and solid inorganic electrolytes have gained a lot of attention. Glass and ceramic electrolytes among this category are gaining importance. Extensive research in the synthesis techniques, cell design and compositions are currently being studies and reported.

Solid-state batteries offer the following properties:

(1) Long shelf life
(2) No gassing
(3) High energy density
(4) Broad operating conditions (-40 to 170˚C for Li anodes & >300˚C for other anodes)
(5) High volumetric energy density
(6) Shock and vibration-resistant

However, the solid state batteries have certain disadvantages such as

(1) Low current drains
(2) Low power densities

There are both pros and cons offered by the solid inorganic electrolytes. The main disadvantage of this type is the low conductivity of various inorganic solid electrolytes ranging between 10^{-4} to 10^{-8} S/cm at room temperatures. The electrode-electrolyte interface is just another important factor for consideration. Although the glass ceramic electrolytes have significantly high conductivity at room temperature (~10^{-3} S/cm), contact resistance with the electrode is very high. This hinders the use of the solid state battery in HEV, EV applications. Hence, proper adhesion between the solid electrolyte and electrode need to be studied to get better cycleabilty.

The solid electrode volume expansion during intercalation/de-intercalation of lithium ions is another factor to affect the performance of solid state LIBs. Even though electrolytes that have high conductivity ~ 10^{-3} S/cm at room temperature are used, the solid state battery is not capable of charging and discharging after the first cycle. This can be attributed to the fact that significant volume expansion affects the contact between active material particles and solid electrolyte.

1.4.2 Crystalline Ceramic Electrolytes

More than 20 different compositions of the polycrystalline lithium electrolytes with perovskite crystalline structure are reported in the previous years. The highest reported conductivity was $1.5X10^{-3}$ S/cm for $La_{2/3-x}Li_{3x}TiO_3$ at x~0.11[40]. Most of the perovskite electrolytes are synthesized by solid state reactions and pressed and sintered to make pellets. This so-called Nasicon phase (Na SuperIonic Conductor) is another class of ceramic electrolyte that has been extensively studied. The general composition is $Li_{1+x}M_2(PO_4)_3$ with $0<x<3$. Different compositions by varying the metal ion in the electrolyte have been studied. The structure consists of PO_4 and MO_6 polyhedra associated at corners to form 3D tunnels in the crystal. Originally, sodium containing Zr as metal was researched. Conversely using Ti seemed to be better, resulting in conductivity of 3 mS/cm. Although Ti^{4+} has limited applications because of its reducibility, other compositions such as Al, Ta, or Ge seemed to have high expectations. A composite electrolyte using Al and Ti was synthesized using $LiBO_2$, LiF additive to block the electronic conductivity. The authors successfully characterized the $Li_4Ti_5O_{12}/LiMn_2O_4$ battery using the composite electrolyte [41]. Although the battery was successfully prepared and cycled, good performance couldn't be achieved.

In latest publications, reports of synthesis of glass-ceramic lithium electrolytes are found, wherein the ceramic phase has the Nasicon-type crystal structure. Sintered ceramics of the compositions of Al, Ti, and Ge are already studied [42]. These solid electrolytes have high conductivities. The benefits of such a solid electrolyte include:

- Ease of manufacture
- Low grain boundary resistance
- Thick and dense microstructure

The sintering temperature was increased to lower the activation energy as well as enhanced conductivity due to grain growth. The Lisicon-type solid electrolytes are referred as 'Lithium superionic conductors'. The general composition is ABO_3 and the crystalline structure is known as ΥLi_3PO_4. The B tetradedra share corners with clusters of three AO_4 tetradedra. Most typically the A sites are Li and Zn, while the B sites are V and Ge, forming

solid solutions by mixing the A and B cations[43]. The first composition studied in this series is the solid electrolyte with composition of $Li_{3.4}$ ($V_{0.6}Si_{0.4}$) O_4. As a bulk material, the solid electrolyte has good ionic conductivity of 1 mS/cm and low electronic conductivity of $t_e \sim 10^{-7}$. However, when used as a thin film the electronic conductivity increased with side self-discharge currents. This was due to the large surplus of Li_2O deposited in the highly disordered material that conceded the electronic conductivity of the solid electrolyte [44].

New kinds of solid electrolytes are being investigated referred to as 'thio-lisicon solid electrolytes'. Solid state cell composed of In/$LiCoO_2$ with the more resistive Ge, Ga electrolyte exhibits an initial discharge capacity of ~ 80mAh/g at low C-rate. Further research and development need to be put in analyzing this kind of solid electrolyte. Other kind of solid electrolyte compositions of lithium metal halides, nitrides and phosphides are being investigated. Even though some of the solid electrolytes seem promising in certain areas, none of the studies has advanced to the point of testing electrochemical cells or forming the electrolyte as a thin layer.

1.4.3 Overview of Ceramic Polymer Solid Electrolytes

Reports in the literature already prove that Ceramic solid electrolytes are known to have high conductivity even at room temperature. However, when used as solid electrolyte in the cells, they have high interfacial resistance with the other components of the battery. Hence as already discussed in the previous section, when the ceramic solid electrolytes are used in conjunction with polymers, the prepared composite could be highly promising.

NASICON type, lithium super ion conducting ceramic for $Li_{1+x}Al_xTi_{2-x}(PO_4)_3$ (LATP) at x~0.3 exhibits maximum conductivity of ~ 10^{-3} S/cm at 300K . Yet, when tested in a symmetric cell using $LiMn_2O_4$ as the electrode, the electrochemical performance of the cell was poor [45]. This could be attributed to the high interfacial resistance between

the components of the cell. The main factor contributing the poor performance is the interfacial resistance between the electrode/electrolyte.

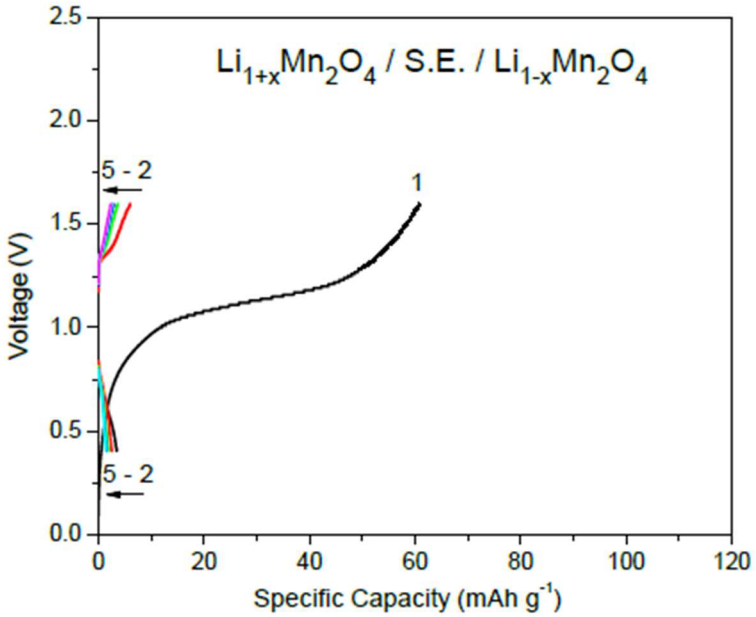

Figure 1.7 Electrochemical performance of the all solid state cell at 25 μA [45]

At a slow current rate of 0.1 mA/cm^2, a smooth charge curve with an initial capacity of 60 mAh/g was reported. However, the subsequent cycles showed negligible capacity. The primary problem was attributed to the high interfacial resistance and the volume change accompanied by the intercalation/de-intercalation of the Li ions in the $LiMn_2O_4$ electrode.

Thus, compositing the ceramic solid electrolyte with a suitable polymer binder could help in tackling the above mentioned problem. Several ion conducting polymers have been the focus of much research in the past few years. To use the polymer electrolytes in the lithium batteries, the ideal polymer needs to exhibit the following properties:

- Adequate conductivity
- High cation mobility

- Mechanically stable
- Good interfacial contact with electrodes
- Wide electrochemical stability
- Chemical & thermal stability
- Safe
- Ease of processing

Although not all the properties could be seen in a single polymer material, different types are studied which possess most but not all of the desired properties. The commonest polymer electrolyte studied is polyethylene oxide (PEO), which is found at reasonable cost in pure state. Wright et al. was the first to successfully use PEO that dissolved alkali salts to provide ionic conductivity [46]. Fig shows mechanism of dissolution of alkali salts by PEO. By complexing the metal ions through binding interactions between the ether oxygens and the metal ions, the salts are dissolved in PEO. From the Figure 1.7, it could be understood that the conductivity of the material will be higher if the concentration of the charged species is higher. Thus the use of large anions such as bis(trifluoromethysulfonyly) imide ($(CF_3SO_2)_2N^-$), referred as TFSI or imide could reduce the ion-pair binding strength. This helps to delocalize the negative charge over the anion structure. The ionic conduction of the lithium ions occurs by the segmental motion through the amorphous phase of the polymer electrolyte. Since the polymers are mostly crystalline at room temperatures, good conductivity was observed only at elevated temperatures.

Hence, a rule of thumb was utilized for the design of the polymer electrolyte, to reduce the T_g (Glass Transition Temperature) thus eliminating the crystallization of the polymer. At elevated temperatures, there is rapid segmental motion. However, regrettably, at high temperatures the mechanical flexibility of the polymer material is lost, which is required to fabricate practical materials that act as electrolytes as well as separators.

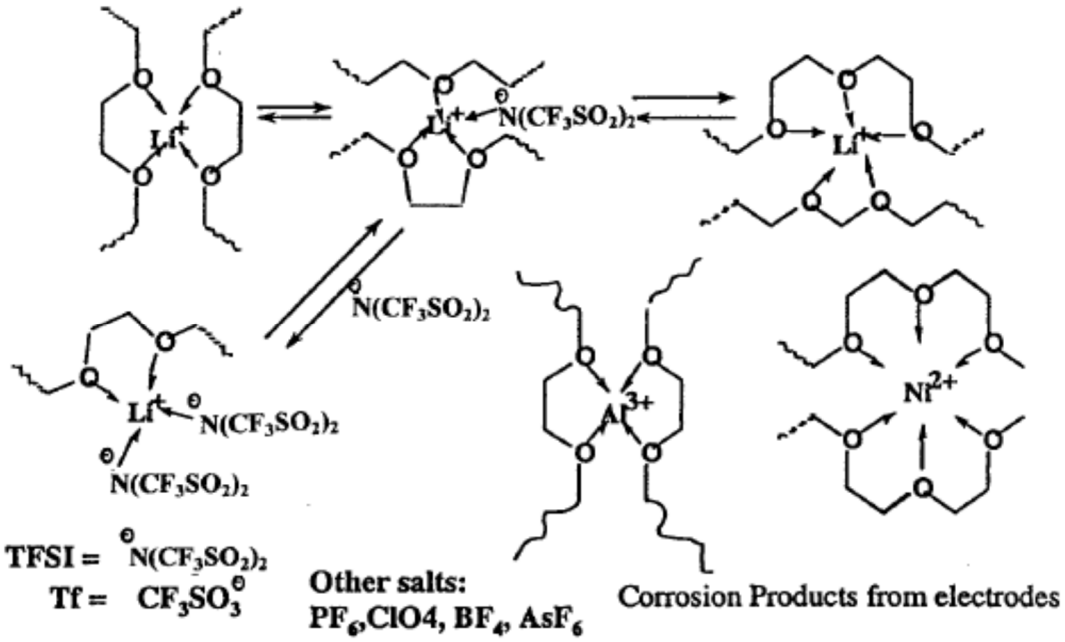

Figure 1.8 Mechanism of dissolution of alkali salts by PEO [46]

Therefore, mechanically hard, single-ion electrolyte particles of ceramic electrolytes could be added to the polymer to form composite solid electrolytes that could offer the advantages of using both as an electrolyte and as separator.

1.5 Objectives

The objectives of the thesis are listed below.

1. Development of synthesis methods for lithium manganese phosphate nano particles with carbon coating. In this study, two different synthesis techniques, solid-state and sol-gel technique are utilized synthesize $LiMnPO_4$ and $LiMn_{0.4}Fe_{0.6}PO_4$ cathode materials.

2. Development of a ceramic - polymer composite solid electrolyte for all solid LIB applications.

2 IMPROVING ELECTROCHEMICAL PROPERTIES OF POROUS $LiMnPO_4$ BY A MODIFIED SOL-GEL PROCESS

2.1 Overview

A great consideration was given in recent years to ortho lithium transition metal phosphates for lithium ion battery cathode materials. This is because of the various advantages that are offered when compared to conventional cathode materials such as low toxicity, chemical and thermal stability and low cost. Padhi and Goodenough did the groundbreaking work in 1996 [47]. $LiFePO_4$ was the first one to be investigated. Exhilarated by its success, $LiMnPO_4$ has increased attention recently.

The potential of $LiMnPO_4$ is higher than $LiFePO_4$, about ~1.65 times. However, because of its intrinsic properties LMP offers high ionic and electronic resistance, making it unsuitable for practical use. Since then several groups have tried to achieve good electrochemical performance in LMP. To overcome the disadvantages presented by LMP, effective approaches were to reduce the particle size to enhance lithium ion diffusion [48] and add carbon coating to improve the electrical conductivity [49-51].

Conversely, optimization of LMP synthesis route can improve the electrochemical performance [52]. Hence, to encounter the problem of Mn dissolution in the electrolyte a modified sol-gel process is adopted.

2.2 Experimental

To compare the effect of synthesis, two different techniques were implemented to prepare LMP cathode particles. The first one is a solid-state route and the second one is a modified sol-gel route.

2.2.1 Solid State Route

The stoichiometric weights of the starting materials Li_2CO_3, $Mn(COOCH_3)_2.4H_2O$, $NH_4H_2PO_4$, ACB are taken in proper proportions are mixed using a dry ball milling process for 10h. The resulting powder is calcined in a flowing N_2 atmosphere at 550˚C for 10h. After the first heat treatment, sucrose is added to the powder and is ground well. Then the powder is subjected to a second heat treatment at 700˚C for 5h. Thus, the LMP-SS ($LiMnPO_4$ by Solid State) cathode powder is prepared.

2.2.2 Sol-Gel Route

The stoichiometric weights of the starting materials Li_2CO_3, $Mn(COOCH_3)_2.4H_2O$, $NH_4H_2PO_4$, and citric acid are dissolved in D.I(distilled) water at room temperature. After homogenously mixing using a magnetic stirring, sol is prepared. Then the gel state is prepared by simultaneously magnetically stirring and heating at 80˚C-90˚C. After all the water is completely removed, it is calcined at 700˚C for 10h in N_2 atmosphere. Sucrose is added to the powder in D.I water and again sol and gel state are prepared as mentioned above and finally calcined in N_2 atmosphere at 700˚C for 5h. Thus, the LMP-SG ($LiMnPO_4$ by Sol Gel) cathode powder is prepared.

Two sets of cathode were prepared by grounding LMP powder, super-P carbon black (Alfa) and poly (vinylidene fluoride) (PVdF) binder in 80:10:10 ratio in N-methylpyrrolidone (NMP). The resulting slurry was casted on aluminum foil and dried at 95˚C for 12 h to remove solvent.

Circular discs of ~ 0.50 cm^2 and mass- 3 mg were cut for electrochemical testing. A typical 2 – electrode coin cell was fabricated using 1M $LiPF_6$ in EC/DMC (1:1 vol.%, Samsung Co.) electrolyte and Celgard®-2200 as a separator. Cell assembly was performed under argon atmosphere in a glove box (H_2O, O_2 < 0.1 ppm).

2.3 Characterization Techniques

To analyze the crystallographic structure of LMP, X-ray power diffraction (XRD) is done. This was carried out by a SIEMENS D5005 X-ray diffractometer using CuK_α radiation (35Ma/40Kv) and a graphite monochromator. The data was collected in the 2θ range of 15-120˚ with 0.02 step interval and 10s step time. To minimize any preferred orientation and statistical errors in calculation the sample was rotated at 30 rpm.

Scanning electron microscopy (SEM) imaging was carried out with FE-SEM (Philips XL30 S FEG). The dissolution of Mn in the electrolyte and the chemical composition of active materials were determined using inductively coupled plasma (ICP) analysis (Atom scan 25, Optima 4300DV). The carbon content in the electrode was determined from elemental analysis (CHNS-932, LECO).

2.4 Results and Discussions

Figures 2.1 & 2.2 present the XRD patterns of $LiMnPO_4$ synthesized by two different techniques. The XRD crystallography of $LiMnPO_4$ by both the solid state and sol gel routes, confirm the formation of $LiMnPO_4$. From the XRD patterns, it can be known that the material is orthorhombic with crystalline particles. No impurities were detected, indicating that with the synthesis routes pure $LiMnPO_4$ can be synthesized [53].

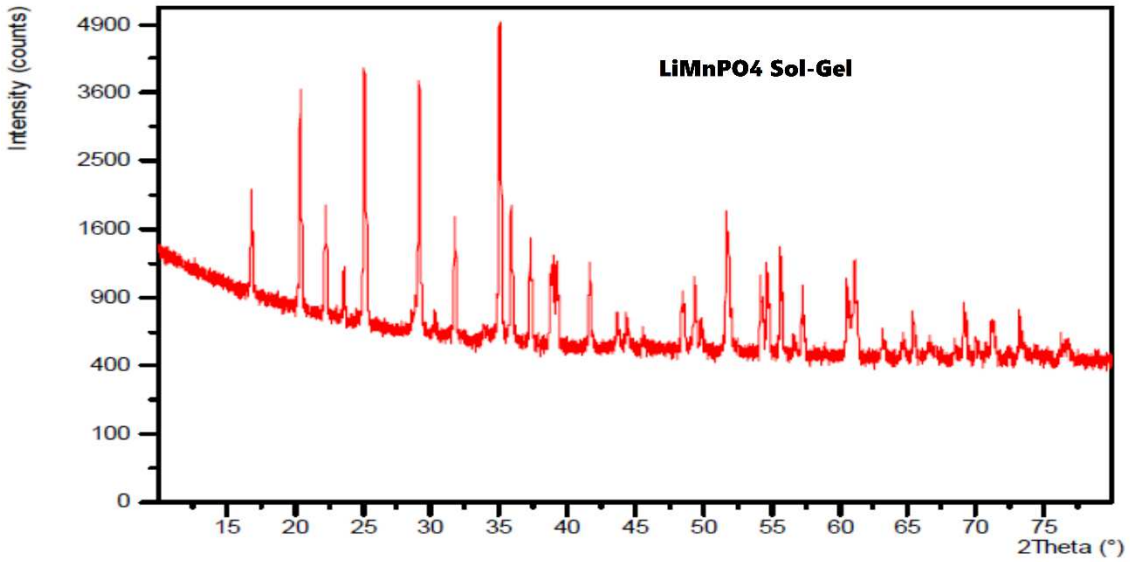

Figure 2.1 XRD pattern of $LiMnPO_4$ by sol-gel technique

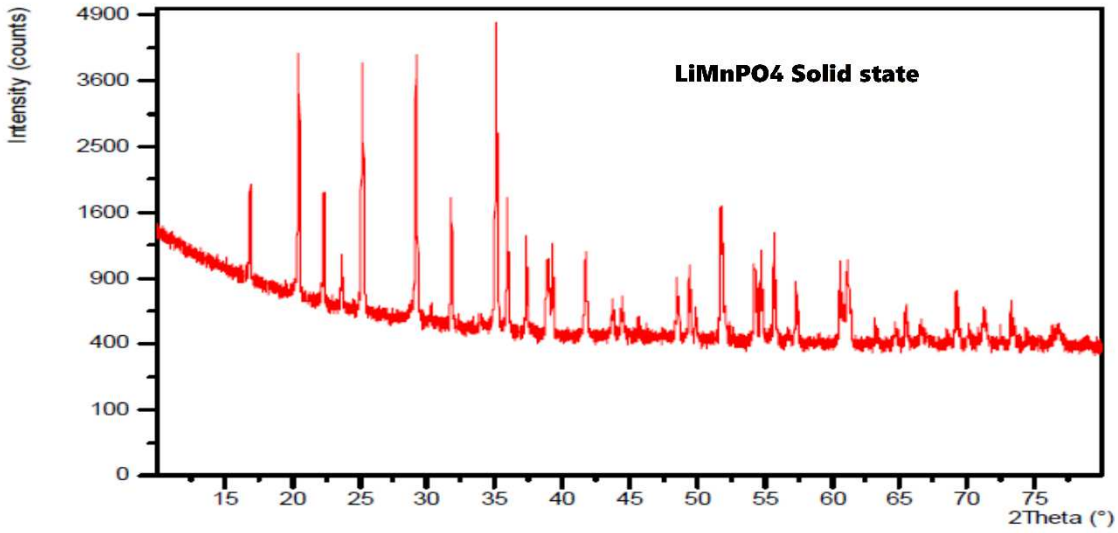

Figure 2.2 XRD pattern of $LiMnPO_4$ by solid state reaction technique

Figure 2.3 shows the combination XRD of $LiMnPO_4$ synthesized by two different routes. It is evident from the pattern the consistency obtained by the two different routes. In addition, the crystallographs agree well with the literature [53].

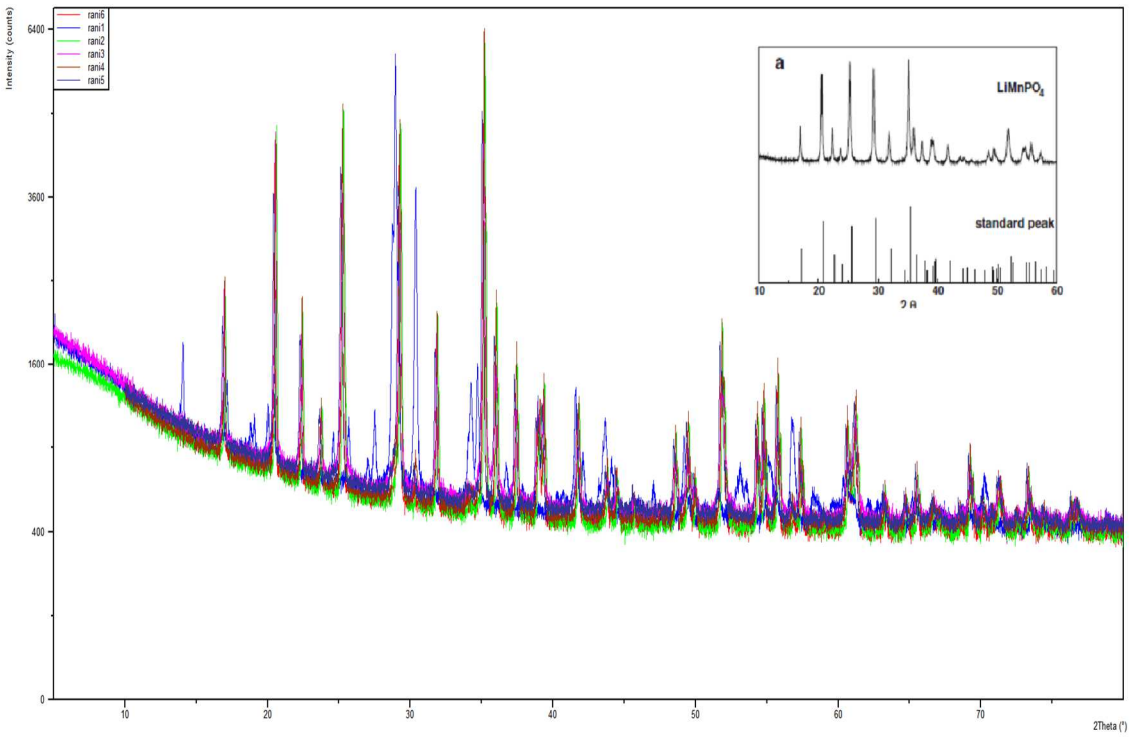

Figure 2.3 Combination XRD of solid state and sol gel synthesis routes

From the XRD patterns of the $LiMnPO_4$ /C samples, all the samples can be indexed to the orthorhombic *Pnma* space group structure (PDF # 74-0178) based on a well-ordered olivine structure.

No diffraction peaks of carbon in the crystalline state can be detected. This means that all the carbon is present in the amorphous state.

The carbon content in the sample of the $LiMnPO_4$ /C was verified using elemental analysis. The difference in the carbon wt.% before and after burning the sample to remove all the carbon matched the required 10 wt. % of carbon.

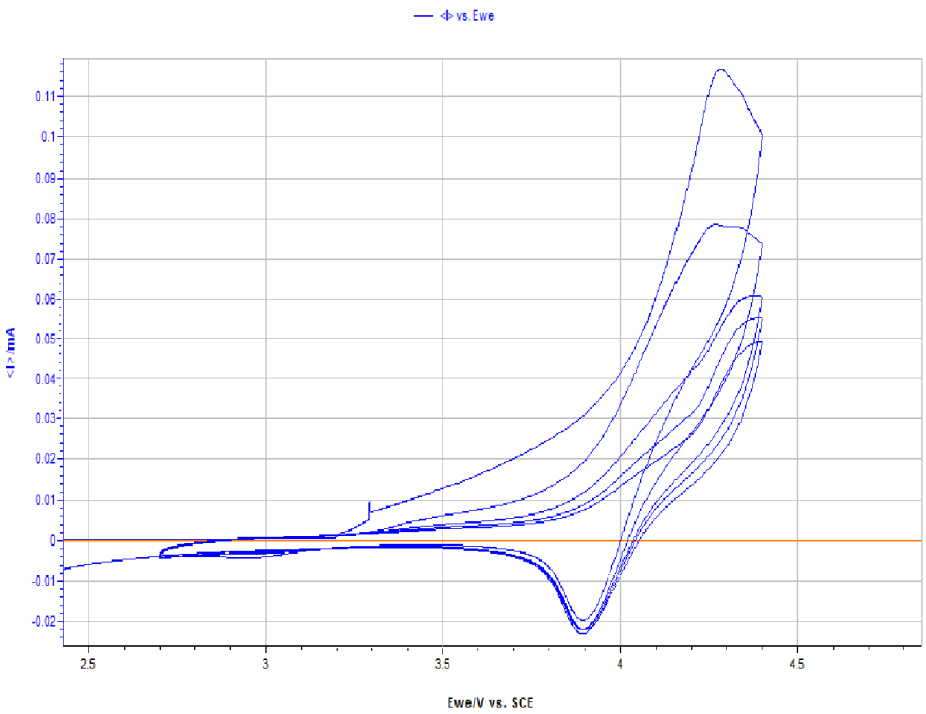

Figure 2.4 Cyclic Voltammograms of $LiMnPO_4$ /C samples

The CV measurements for the prepared $LiMnPO_4$ /C electrode were performed to characterize its electrochemical reactions reversibility in half Li-ion cells. Figure 2.4 shows the typical cyclic voltammograms of the LiMnPO4 /C electrode. The cyclic voltammetry was performed at the scan rate of 0.1 mV/s for 5 cycles. From the voltammograms it can be clearly seen that only a few of the cathodic and anodic peaks appear at 3.9 V and 4.35 V at 0.1 mV/s scan rate. The peak positions are different for the CV curves measured at different cycles, also the difference of the peak separations between the anodic and cathodic peaks increases very much as the cycles progresses.

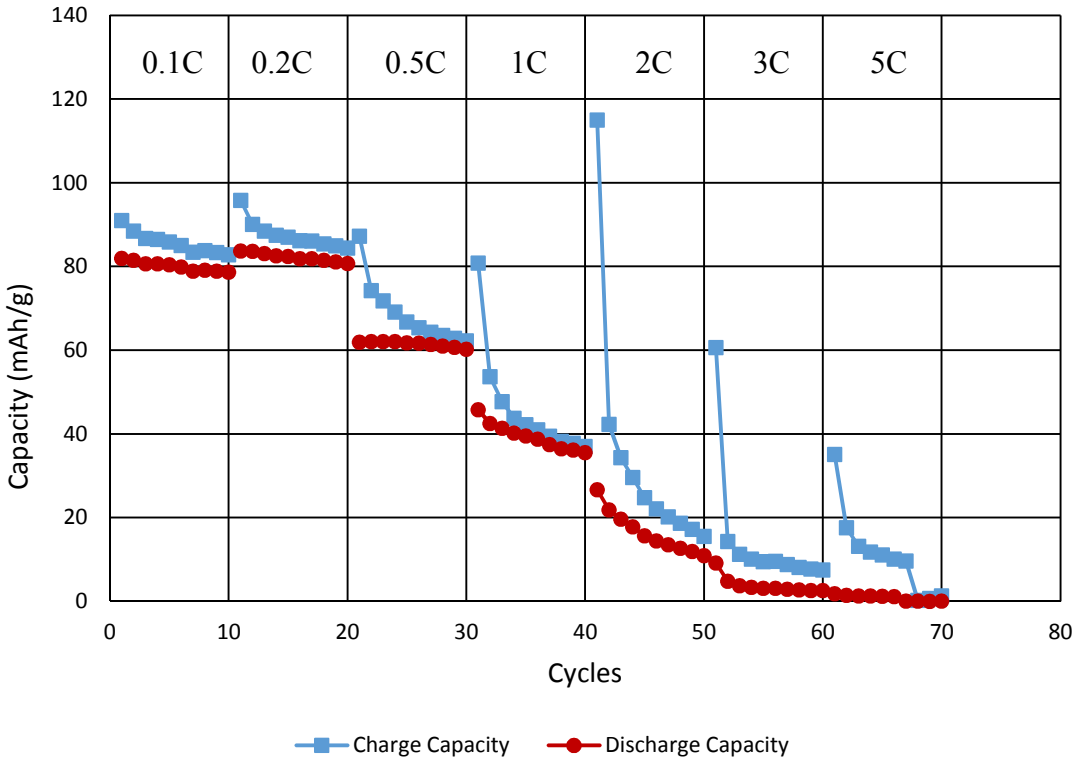

Figure 2.5 Short-term cycling of $LiMnPO_4$/C at different C-rates (0.1 C, 0.5 C, 1 C, 2 C, 3 C, 5 C)

To estimate the rate-capability of the prepared $LiMnPO_4$ /C electrodes, the cells were cycled between 2.7 V to 4.4 V at 0.1 C, 0.5 C, 1 C, 2 C, 3 C, 5 C rate. Figure 2.5 shows the charge-discharge curves of the $LiMnPO_4$ samples at different C-rates. The charge capacity of the sample for the first cycle at 0.1 C was 89 mAh/g, which is around 60% of theoretical capacity. When the current density was increased, the capacity of $LiMnPO_4$ /C decreased. When the current density increases to 0.5 C, 1 C, 2 C, 3 C and 5 C, the charge capacity of the samples were 90, 74, 80, 42, 17, 14 mAh/g; while the discharge capacity were 81, 83, 61, 46, 26, 4, 2 mAh/g respectively. The specific capacity during charging is higher than that obtained for discharge, however, this difference gradually decrease with increasing cycle number because of the stabilization of solid electrolyte interface (SEI) layer on surface of anode. The active material surface area, the

uniform pore size distribution, as well as the nature and effectiveness of the conductive coating, are crucial factors that have an influence on the electrochemical performance.

To evaluate the cycle performance of the $LiMnPO_4$ samples, the cells were cycled for 100 cycles at 0.1 C, 1 C rate. Figure 2.6 shows the electrochemical characteristics of the $LiMnPO_4$ at 0.1 C and Figure 2.7 shows the charge/discharge characteristics at 1 C rate. Even though the number of Li ions extracted from the cathode is not high, the capacity retention rate of the $LiMnPO_4$ /C samples were stable.

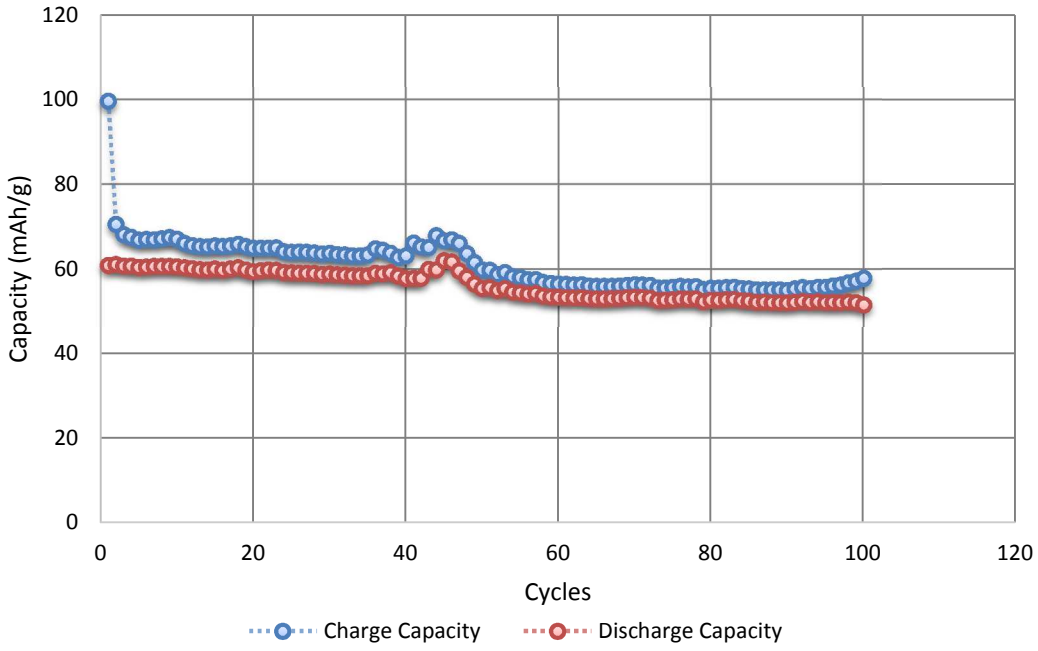

Figure 2.6 Cyclic Behavior of $LiMnPO_4$ at 0.1 C by Sol-gel Technique

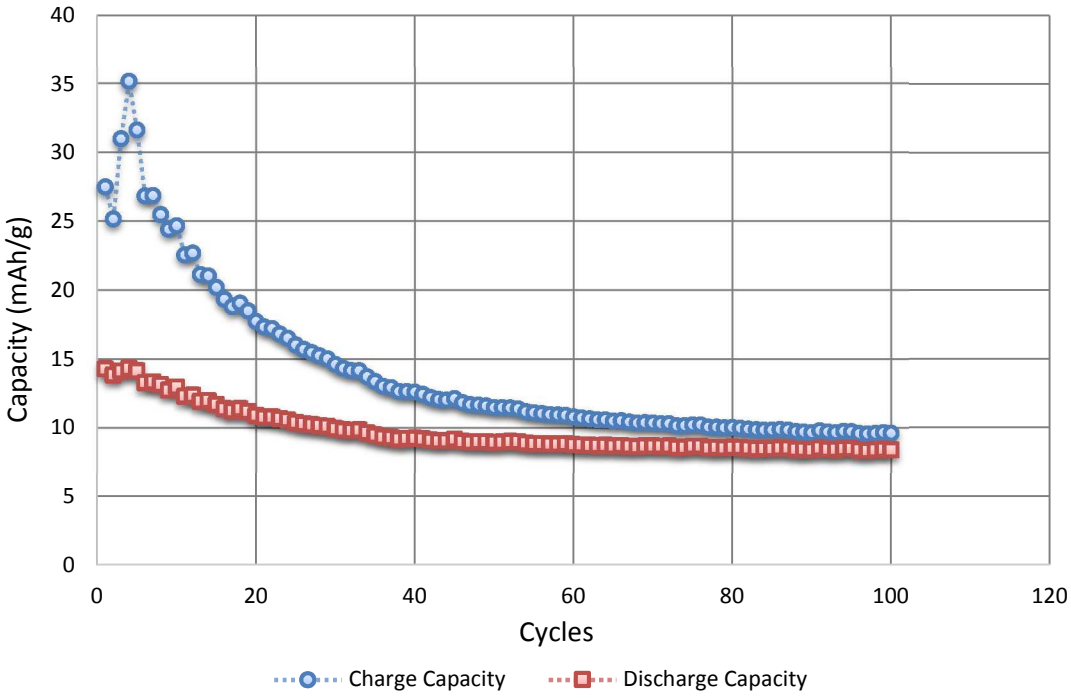

Figure 2.7 Cyclic Behavior of $LiMnPO_4$ by Sol-gel Technique at 1 C rate.

Even at 60˚C as shown in Figure 2.8, the samples exhibited good capacity retention rate. However, the number of moles extracted from the $LiMnPO_4$ electrode was less during the charge process. The reduction in the capacity of the samples can be attributed to the presence of agglomerated primary particles and heterogeneous carbon coating. Due to this issue, the electrical resistance increased and the lithium insertion and extraction process was poor. Thierry Drezen et al. proposed that as the particle size of the active material increases, lithium diffusion becomes gradually difficult due to both the lithium diffusion of Li^+ within a single large particle and the difficulty of electron transport through the bulk of the material [54].

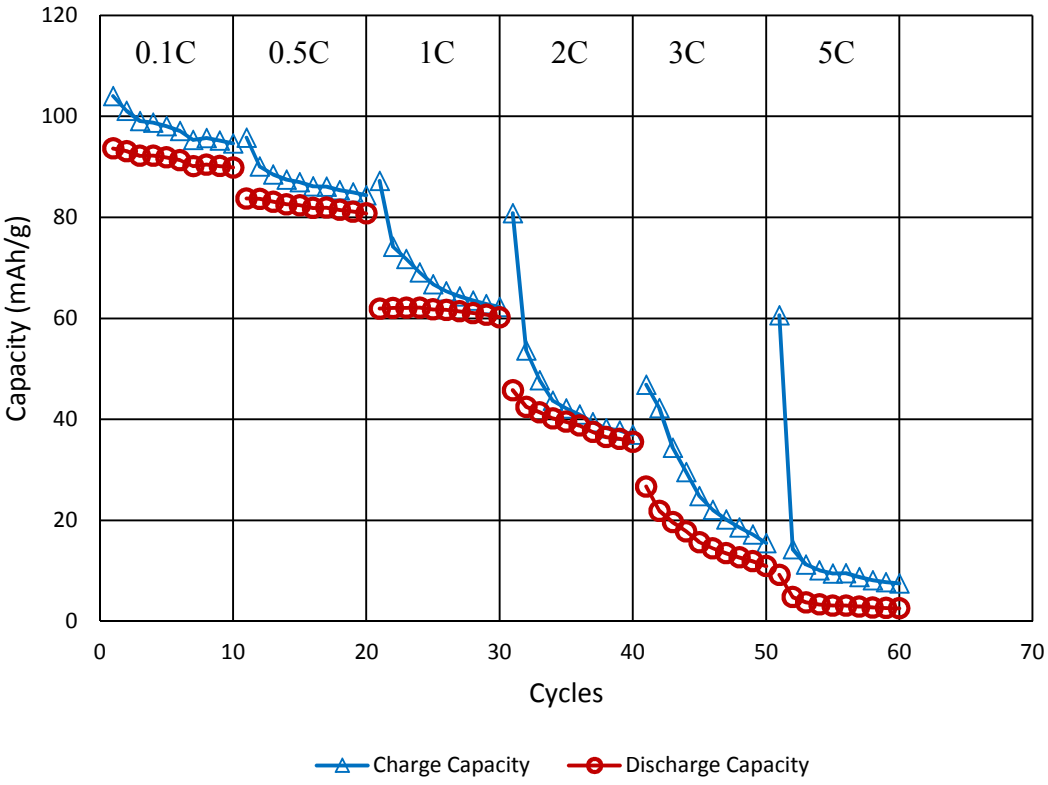

Figure 2.8 Short-term cycling of $LiMnPO_4$/C at different C-rates at 60˚C

2.5 Summaries

A lot of focus was put in achieving optimal properties of olivine type cathode material $LiMnPO_4$ in the past few years. The problems associated with this cathode material are its intrinsic insulating properties and Mn dissolution in the electrolyte. The synthesis technique was proven a vital factor in realizing optimal performance of $LiMnPO_4$. Using a modified sol-gel technique, $LiMnPO_4$ nano-particles are synthesized and the electrochemical characteristics were studied.

3 CHAPTER-THREE: IMPROVING ELECTROCHEMICAL PROPERTIES OF POROUS $LiMn_XFe_{1-X}PO_4$ (X = 0.6) IN ADDITIVE ADDITION ELECTROLYTE

3.1 Overview

With the success of Padhi *et al* [55] in 1997 to show reversible electrochemical lithium insertion-extraction in $LiFePO_4$, much focus was put on olivine compounds as $LiFePO_4$ and $LiMnPO_4$. Because of their suitable structure, the additive-olivines are extremely safe at high temperatures [56] and abusive conditions [57].

The system of Mn doped with $LiFePO_4$ looks encouraging as this system operates at a voltage range of 3.4-4.1 V vs Li/Li^+[58].Since then different groups have studied to improve the performance of this system[59].

By developing a porous cathode of $LiMn_{0.4}Fe_{0.6}PO_4$ by a modified sol-gel process, the capacity and energy density were achieved, the cycle life was poor. This is due the Mn dissolution in the electrolyte. This problem was overcome by the addition of tris (trimethylsily) phosphite TMSP additive in the electrolyte.

3.2 Experimental

$LiMn_{0.6}Fe_{0.4}PO_4$ was prepared by a modified sol-gel process, in which the starting materials used are Li_2CO_3, $FeC_2O_4{\cdot}2H_2O$, $Mn(COOCH_3)_2{\cdot}4H_2O$ and $NH_4H_2PO_4$ (All 99%, Aldrich) and citric acid (Shinyo Pure Chemicals, 99%). Li_2CO_3, $FeC_2O_4{\cdot}2H_2O$, $Mn(COOCH_3)_2{\cdot}4H_2O$ and $NH_4H_2PO_4$ were dissolved in triple distilled water at room temperature to which citric acid solution was added slowly. After the solution was mixed homogenously, it was dried at 80˚C for 12h. The formed wet gel was again heated at

70˚C for 12 h in vacuum oven. The resulting product was fired at 700˚C for 10 h to prepare $LiMn_{0.6}Fe_{0.4}PO_4$.

The cathode was prepared by grounding $LiMn_{0.6}Fe_{0.4}PO_4$ powder, super-P carbon black (Alfa) and poly (vinylidene fluoride) (PVdF) binder in 80:10:10 ratio in N-methylpyrrolidone (NMP). The resulting slurry was cast on aluminum foil and dried at 95˚C for 12 h to remove any solvent.

Circular discs of 0.95 cm^2 and mass ~3.0 mg were cut for electrochemical testing. A typical 2 – electrode coin cell was fabricated using 1M $LiPF_6$ in EC/DMC (1:1 vol. %, Samsung Co.) electrolyte and Celgard®-2200 as a separator. A 1 wt.% of Tris (trimethylsily) phosphite was used as an additive. Cell assembly was performed under argon atmosphere in a glove box (H_2O, O2 < 0.1 ppm).

3.3 Characterization Techniques

To analyze the crystallographic structure of LMFP, X-ray power diffraction (XRD) and Rietveld refinement is done. This was carried out by a SIEMENS D5005 X-ray diffractometer using CuK_α radiation (35Ma/40Kv) and a graphite monochromator. The data was collected in the 2θ range of 15-120˚ with 0.02 step interval and 10 s step time. To minimize any preferred orientation and statistical errors in calculation the sample was rotated at 30 rpm. Using the FullProf program crystal structure refinement in the space group *Pnma* was done. Scanning electron microscopy (SEM) imaging was carried out with FE-SEM (Philips XL30 S FEG). Brunauer–Emmett–Teller (BET) method was utilized to measure the specific surface area in the N2 sorption data of ASAP 2020 Analyzer. The dissolution of Mn in the electrolyte and the chemical composition of active materials were determined using inductively coupled plasma (ICP) analysis (Atom scan 25, Optima 4300DV). The carbon content in the electrode was determined from elemental analysis (CHNS-932, LECO).

3.4 Results and Discussions

XRD pattern of $LiMn_{0.6}Fe_{0.4}PO_4$ (LMFP) reveals a standard orthorhombic olivine structure that is consistent with PDF card No. 40-1499. No impurities were seen, suggesting that high purity LMFP could be synthesized by typical sol-gel process.

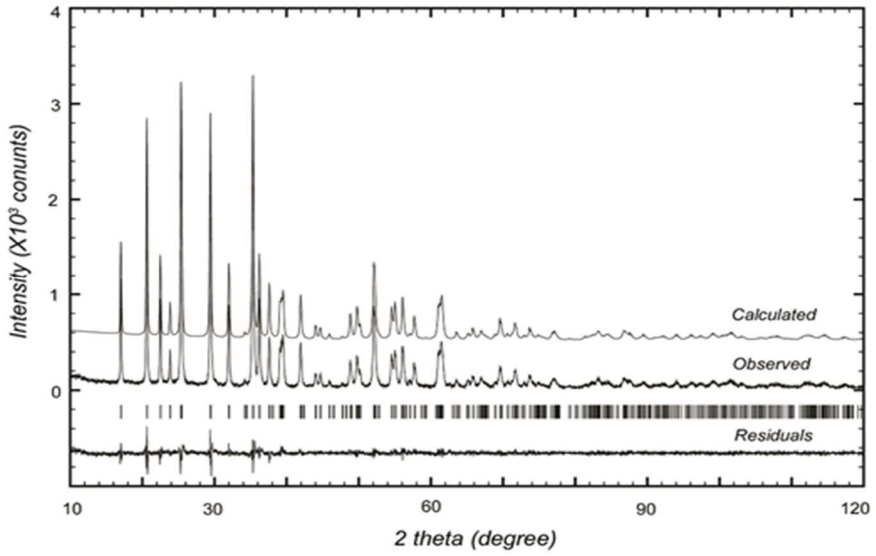

Figure 3.1 X-ray diffraction pattern and Rietveld refined result

From the XRD data as shown in Figure 3.1, the peak intensity ratios are 1.01 and 0.97 suggesting the distortion of the crystal lattice of $LiFePO_4$ due to Mn atoms. The LiO_6 octahedra structure in LMFP form edge-sharing chains with the b-axis, and along this axis Lithium ion transport is carried out in zig-zag pattern between adjacent Li sites [60]. The effective cross sectional area and the space of triangular LiO_6 octahedra face (O_2-O_3-O_1) plays an important role in Li ion diffusion and transport respectively (Figure 3.2). Table 3.1 gives the selected interatomic distance (Å) and angle (°) of LiO_6 obtained from the Rietveld analysis in LMFP structure.

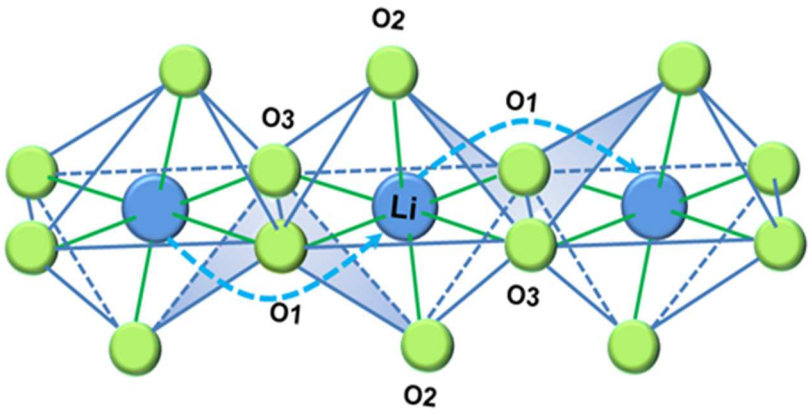

Figure 3.2 Schematic configuration on the LiO_6 octahedra of $LiMn_{0.6}Fe_{0.4}PO_4$

Table 3.1 Selected interatomic distance (Å) and angle (°) of LiO_6 in $LiMn_{0.6}Fe_{0.4}PO_4$

		Bond	LMFP
Li	Distances	(Li)-(O1) x 2	2.192(5)
		(Li)-(O2) x 2	2.092(3)
		(Li)-(O3) x 2	2.157(4)
	Angles	(O1)-(Li)-(O2) x 2	88.1(3)
		(O1)-(Li)-(O2) x 2	91.92(2)
		(O1)-(Li)-(O3) x 2	84.3(3)
		(O1)-(Li)-(O3) x 2	95.7(3)
		(O2)-(Li)-(O3) x 2	70.9(3)
		(O2)-(Li)-(O3) x 2	109.1(3)

Figure 3.3 shows the SEM and TEM micrographs of LMFP. From the micrographs it can be concluded that the cathode structure is highly porous and the surface, pores and

the walls are well coated with carbon. The SEM and TEM micrographs suggest that the particle size range between 200 nm and 12 μm and the average particle size is 3-6 μm. The micron-sized particles are cheese-shaped and have a homogeneous morphology. At higher magnification, the SEM shows that the pores are present on the surface of the particles. The highly porous structure allows the pores to be filled with electrolyte improving the diffusion of lithium ions.

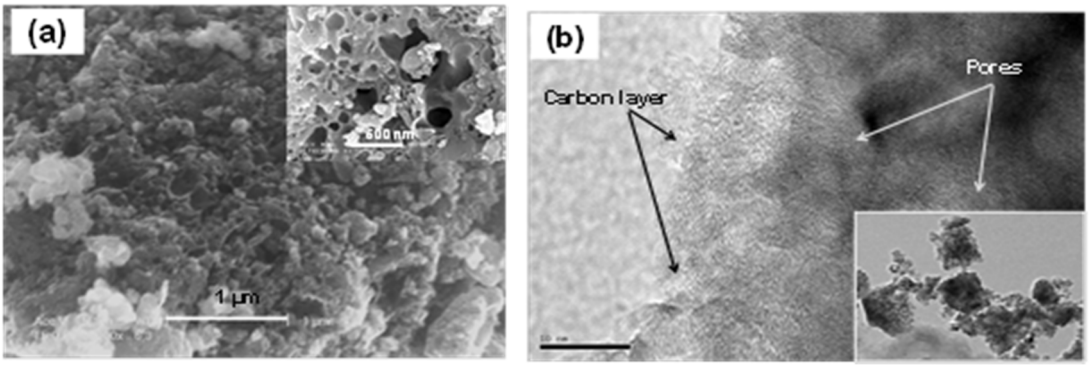

Figure 3.3 (a) SEM and (b) TEM images of carbon coated porous $LiMn_{0.6}Fe_{0.4}PO_4$ particles

A homogenous nano-web of carbon coating is observed through the TEM on the LMFP particles aiding in the Li ion diffusion, charge-transfer kinetics, and increased reversible capacity.

Using BET, the LMFP surface area is estimated as 91.5 m^2/g. The pore size is highly distributed around 64 Å, with a distribution of 10-100 nm.

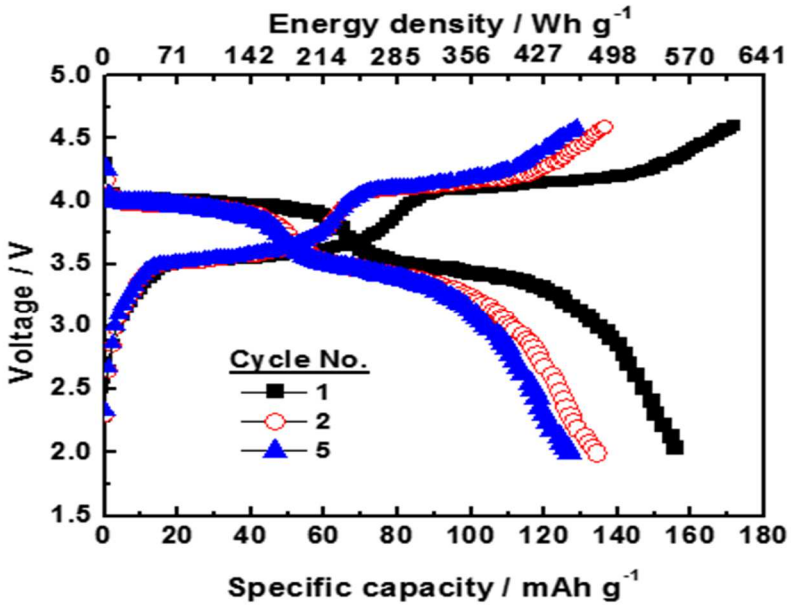

Figure 3.4 First, second and fifth cycles charge-discharge profiles of Li/$LiMn_{0.6}Fe_{0.4}PO_4$ cell in conventional electrolyte (1 M $LiPF_6$ in EC/DMC, 25°C)

The charge- discharge performance at 0.1 C-rate of the LMFP cell delivers an initial discharge capacity of 152 mAh/g, equivalent to 89% of the theoretical capacity (Figure 3.4). The sucrose addition in the sol-gel process during maturing helped to reach high electrical conductivity (1.2 X 10^{-1} S/cm) and hence the higher capacity when compared to typical sol-gel process (134 mAh/g).

Two distinct plateaus in the charge curve at 3.54 and 4.12 V, correspond to the Li ion extraction from LMFP due to Fe^{3+}/Fe^{2+} and Mn^{3+}/Mn^{2+} couples, respectively. This can be supported by the discharge plateaus at 3.48 and 4.0 V corresponding to the former couples respectively. With the increase in the number of cycles, the formation of solid electrolyte interface (SEI) layer assists in the increase of the specific capacity of charging when compared to the discharge specific capacity. As the LMFP particles are highly porous and sub-micron sized, Mn dissolution in the electrolyte would be induced [61]. Choi et al explains that the decomposition of electrolyte produces HF, which attacks the formed SEI

layer, eventually encouraging Mn dissolution of the electrolyte [62]. Hence, the capacity faded with cycle life when a conventional electrolyte (1M $LiPF_6$ in EC/DMC) is used.

To endorse this problem Tris (trimethylsily) phosphite (TMSP) was added as an additive in the conventional electrolyte. This additive not only scavenged the HF, but also formed SEI on the surface of the cathode. The oxidized TMSP eliminated HF produced from the $LiPF_6$ base electrolyte and formed products with P-F group (Figure 3.5) by an electrochemical reaction and also formed SEI with EC [63].

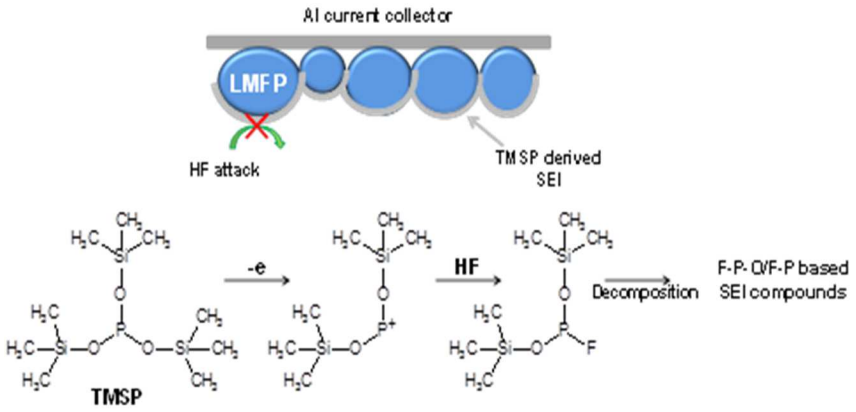

Figure 3.5 Schematic representation of TMSP additive effect and HF scavenging mechanism

This can be proved by the evidence of just 4 ppm of Mn dissolution in the electrolyte with TMSP additive (86 ppm in 1M $LiPF_6$ in EC/DMC) even after 50 cycles.

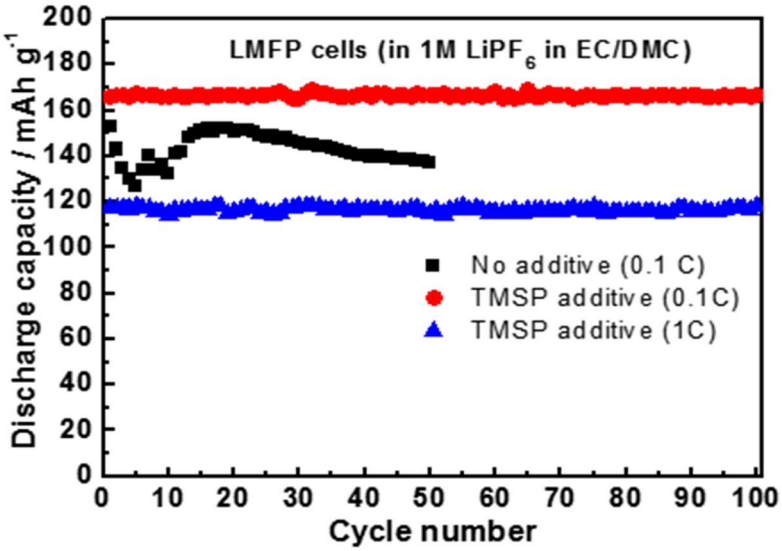

Figure 3.6 Cycle performances of LMFP cells cycled in (1 M LiPF6 in EC/DMC) without and with TMSP additive (1 wt.%)

The charge- discharge performance at 0.1 C-rate of Li/LMFP cells with two electr olytes (with and without TMSP additive) at room temperature is shown in Figure 3.6. The cells with the TMSP additive in the electrolyte displayed higher capacity and stability eve n when cycled to 100 cycles. Comparison of the two electrolytes based on the discharge c apacity of first and 50th cycle exhibited ~ 30 % without additive and ~ 0 % for TMSP addi tive per cycle, respectively. Short cycling performance of the porous LMFP electrode with TMSP additive at different current rates is shown in Figure. 3.7. When the current density is increased to 0.1, 0.2, 0.5 and 1 C, the discharge capacities can maintain at about 153, 136, 119 and 85 mA h g^{-1}, respectively. It is found that the storage capacity is stable at each current rate. When the current rate reverses back to 0.2 C, the cell capacity can recover to the original value immediately, which indicates that the synthesized cathode material owns stability formation even after high rate cycles.

These results confirm that highly porous LMFP with large exposure into electrolyte as cathode electrode material can offer good electrochemical performances.

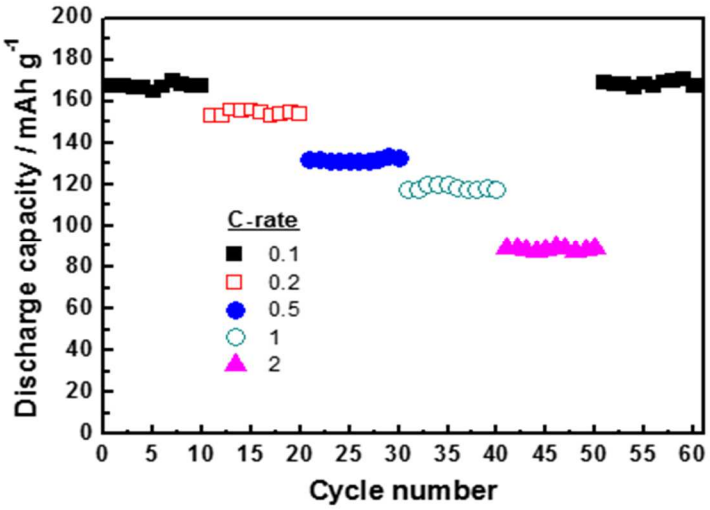

Figure 3.7 Short-term cycling of porous LMFP cell with TMSP at different C-rates (10 cycles at each C-rate, 25°C, 2.0-4.6 V)

3.5 Summaries

A high porous $LiMn_{0.6}Fe_{0.4}PO_4$ composite cathode material was prepared by the modified sol-gel process. The process resulted in the synthesis of micro-sized particles of high specific surface area, surrounded by a uniform and porous web of nanometer sized carbon. The high porosity and homogeneous carbon web provided high lithium ion diffusion and efficient conductivity. A Li/LMFP cell showed a high discharge capacity and energy density of 152 mAh g^{-1} and 570 Wh kg^{-1} at 0.1 C-rate, respectively, as well as an excellent cycling stability with capacity retention ratio of 99% after 10 cycles at all C-rate, and is found promising for large-scale electrochemical applications.

4 DEVELOPMENT OF ALL-SOLID LITHIUM-ION BATTERY USING LI-ION CONDUCTING CERAMICS-POLYMER COMPOSITE ELECTROLYTE

4.1 Overview

Lithium ion batteries have already been developed and commercialized in electric vehicles and other portable electric devices [64]. However, a major challenge has been the safety factor due to the electrolyte leakage, gas formation, explosion, and narrow operating window of voltage and temperature. Extensive enquiry was focused on finding suitable alternatives to address the problems of organic liquid electrolyte. Hence, to realize safe batteries with high energy density an all solid state battery is the one of the suitable solutions. Out of the different kind of solid electrolytes studied like V_2O_5, LIPON, polymer, polymer-gel etc., inorganic solids seemed to be better candidates owing to their high safety and significantly high conductivity. One such material is the fast lithium ion conductive ceramic of NASICON-type $Li_{1+x}Al_xTi_{2-x}(PO_4)_3$ (LATP). At x~0.3 LATP offers high conductivity of ~ 10^{-3} S/cm at room temperature. It is also highly stable in the atmosphere.

Although solid state batteries offer several advantages over liquid electrolyte batteries they couldn't be used for commercial purposes as the battery suffers with poor electrochemical performance. Most of the solid state batteries even at low current rates (<0.07 mA/cm^2) have high capacity fade after the first charge/discharge cycle. One major reason was attributed to the high interfacial resistance between the solid electrolyte and the electrodes. In this study, we propose to develop a ceramic-polymer composite electrolyte to help in resolving the former problem.

4.2 Experimental

4.2.1 Polymer Electrolyte

The polymer electrolyte films of $P(EO)_{10}$-LiTFSI are fabricated by dissolving Polyethylene oxide (PEO) (Aldrich, M.W 6000000 g/mol) and adequate quantities of salt Lithium bis(trifluoromethane sulfonyl) imide (LiTFSI) in dry acetonitrile solution so that the mole ratio of LiTFSI is 10. $P(EO)_{10}$-LiTFSI polymer electrolyte was cast in Teflon dishes. After vacuum drying the polymer electrolyte film was formed. The prepared film was about 250 μm thick. The prepared film was subjected to further tests to investigate its electrochemical performance.

4.2.2 Fabrication of the Ceramic Material

The preparation of the $Li_{1.3}Al_{0.7}Ti_{1.7}$ $(PO_4)_3$ (LATP) was based on literature Aono et al [65]. Lithium carbonate (Li_2CO_3), Aluminum oxide (Al_2O_3), Titanium dioxide (TiO_2), and Ammonium dihydrogen phosphate $(NH_4)_2H_2PO_4$ that were reagent grade were ground and heated in a platinum crucible at 1652˚F for 2 h. The resulting powder was ball milled for 6 h and re-heated at the same conditions. The powder was subjected to ball milling for 12 h to obtain the final LATP powder. The final powder was dried at 120˚C for 24 h to remove any attached water molecules.

4.2.3 Fabrication of the Composite Electrolyte

The LATP powder was mixed with an organic binder of high molecular wt.(~600,000 g/mol) of PEO along with Li salt of LITFSI in different ratios in Acetonitrile solvent to obtain electrolyte slurry. To decrease the crystallinity of PEO and increase lithium ion conductivity, lithium salt LITFSI was added. The slurry was casted on Teflon tape using doctor-blade method. After vacuum drying, solid electrolyte of good flexibility was obtained.

Ionic conductivity was measured at different temperatures for the prepared solid electrolytes of various compositions. After obtaining the best compromise between conductivity and stability, a suitable composition was selected for electrochemical charge/discharge tests.

4.2.4 Fabrication of the Composite Electrode

The positive and the negative electrode were made of the same composition. The electrode slurry was made using Lithium manganese oxide ($LiMn_2O_4$), Super P-carbon (Cnergy), PEO-10LITFSI in Acetonitrile solvent in the weight ratio of 70:10:20. The slurry was coated on Aluminum and Copper foil to produce cathode and anode respectively. To remove the solvent completely it was vacuum dried overnight.

4.2.5 Fabrication of the Battery

The prepared electrode sheets were sandwiched between the electrolytes to prepare an all solid state (A.S.S). To ensure proper contact the layers were pressed together and cut in circular discs. The cell was enclosed in a coin cell for further testing.

To test an all solid state cell with pressure, the circular disc of the cell was placed inside two stainless steel cylinders holed inside an alumina tube. To avoid contact with atmosphere, the space between the stainless steel rods and alumina tube was wrapped with high vacuum grease (Dow Corning Corporation) together with a tape.

Since, LITFSI is highly sensitive to moisture all the experimental part was done inside an Argon- filled glove box with water and oxygen content below 0.1 ppm.

4.3 Characterization Techniques

Confirmation of the crystallographic structure of the LATP was analyzed using SIMENS D5005 X-ray diffractor using CuK_α radiation in the 2θ range of 10-80 with 0.02 step interval and 0.5 s step time. The surface morphology of LATP was studied using SEM.

Electrochemical Impedance Spectroscopy (E.I.S) was done using electrochemical workstation CHI660D. The frequency parameters are from 100 kHz to 0.1 Hz at a voltage of 0.01 V. For ionic conductivity measurements, the composite solid electrolyte was enclosed in a coin cell sandwiched between stainless steel blocking electrodes in a glove box and taken out for further testing. To investigate the electrochemical performance of the prepared A.S.S cells, the cells were tested using MITS Arbin instrument.

4.4 Results and Discussions

The XRD patters of LATP were analyzed using SIEMENS D5005 X-ray diffractometer using CuK_α radiation (35 Ma/40 KV) and a graphite monochromator. The crystallographic structure is shown in Figure 4.1.

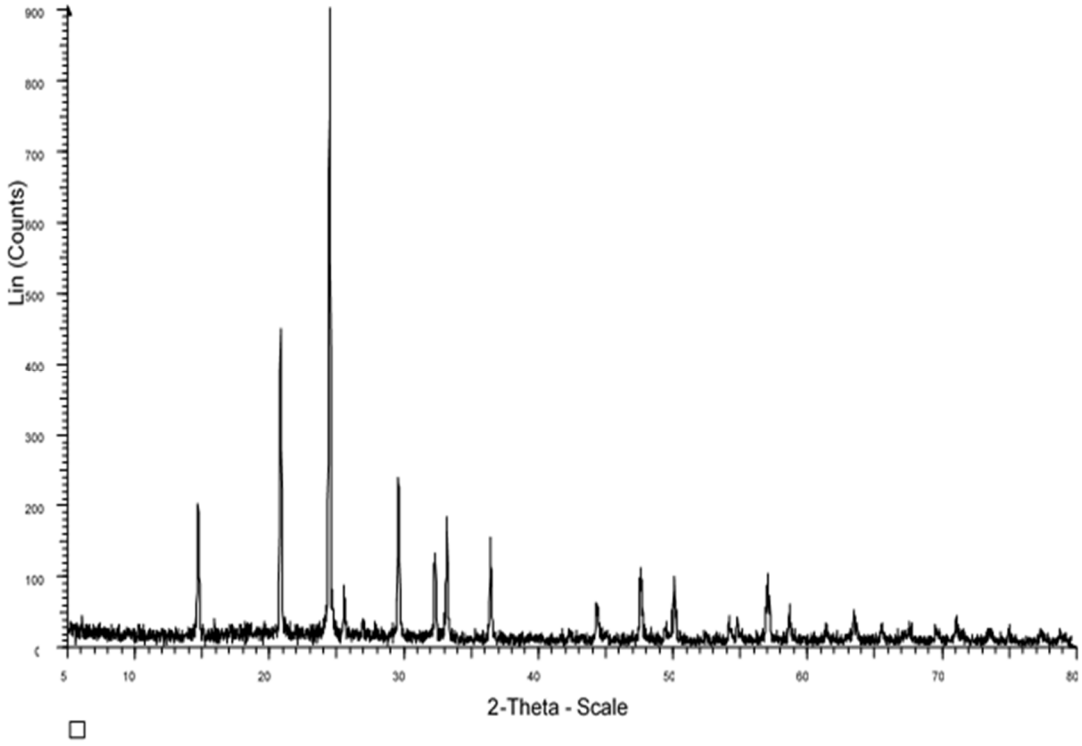

Figure 4.1 XRD of LATP glass-ceramic

The crystallographic structure of the material can be confirmed to that of LATP. A small peak at 26˚ was observed. This may be due to the $AlPO_4$ impurity present, which can often appear at high sintering temperatures [66]. The Al^{3+}ion was merged into the structure of $LiTi_2 (PO_4)_3$ and formed the $Li_{1.3}Al_{0.3}Ti_{1.7} (PO_4)_3$ phase that is the NASICON structure.

SEM photographs of the LATP particles are shown below in Figure 4.2. The SEM pictures of the LATP particles show that the particle size is around 1 μm.

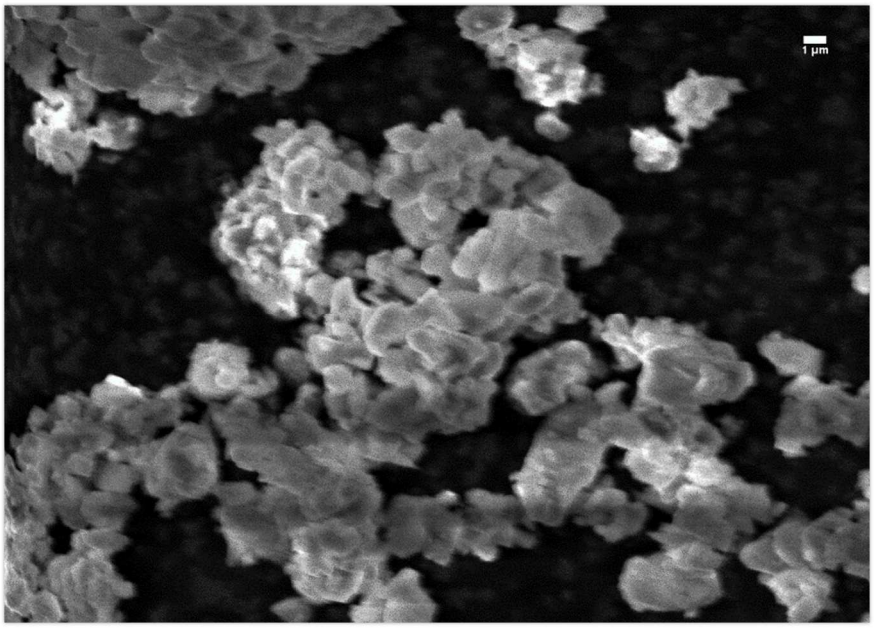

Figure 4.2 SEM of LATP

The most famous polymer has been polyethylene oxide (PEO) with the regular repeat structure $–CH_2CH_2O-$, due to its enormously high solvating properties (maximum concentration > 2 mol dm^{-3}) for a wide range of salts through the interaction of the ether oxygen's with cations. However, at room temperature, this polymer is crystalline, and it is believed that only in amorphous state ionic conductivity is feasible. Hence, focus has been on decreasing the crystallinity of PEO to make it suitable for Lithium ion batteries. Reports in the literature suggest that bulky lithium salts are highly helpful in decreasing the crystallinity of PEO. $LiN(SO_2CF_3)_2$, also referred to as LiTFSI, has been known for the past years for aiding in ion dissociation to delocalize the charge making it favorable to improve ionic conductivity in PEO [67]. Not only does LiTFSI help in improving the conductivity, but also reported to improve the chemical and thermal stability along with providing "plasticizing" effect on the solvating polymer like PEO [68].

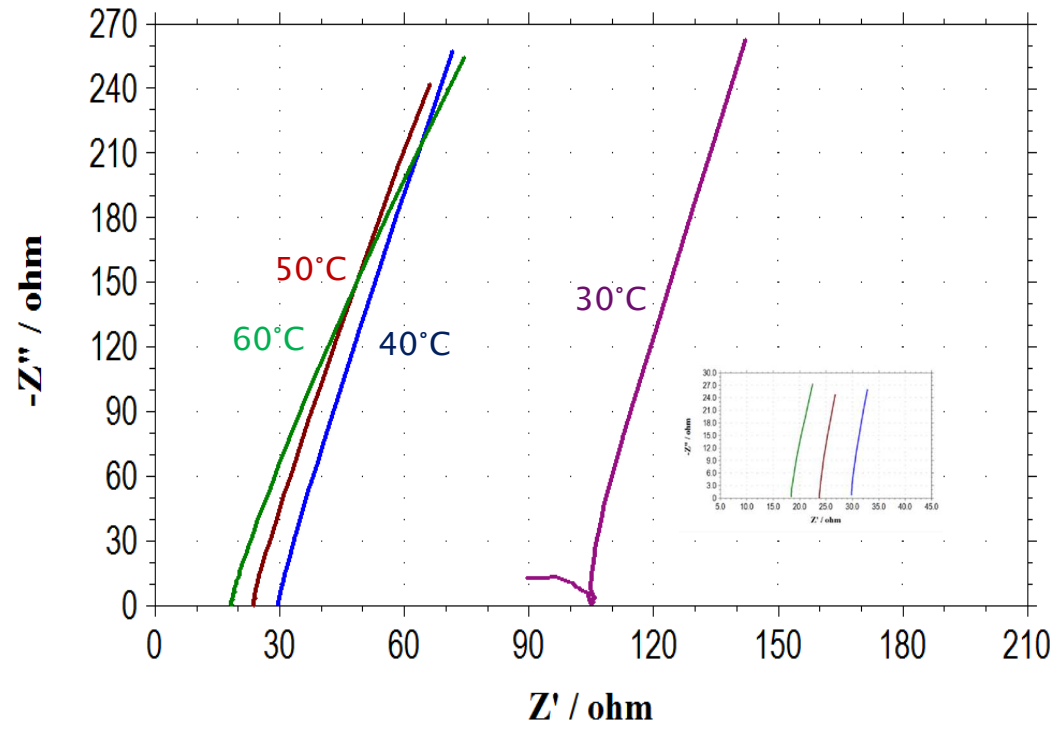

Figure 4.3 EIS plots of polymer electrolyte PEO10-LiTFSI

The electrochemical impedance spectroscopy of the prepared $P(EO)_{10}$-LiTFSI polymer film can be seen in Figure 4.3. The incomplete semicircle is caused by the insufficient upper limit of 100 kHz for electrochemical workstation CHI660A. From the intercept of the inclined line, the conductivity of the polymer electrolyte was plotted at different temperatures as shown in Figure 4.4.

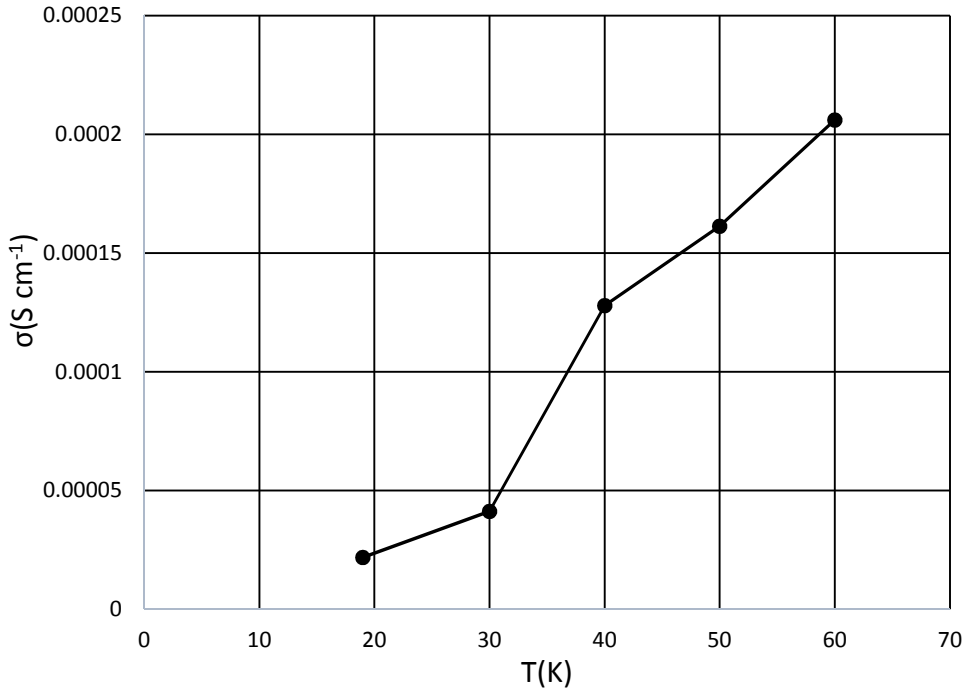

Figure 4.4 Conductivity vs Temperature for the polymer electrolyte PEO10LiTFSI

From the EIS plot it can be seen that the conductivity of the polymer electrolyte matched with the data in the literature for the polymer electrolyte PEO10LiTFSI. It can be understood that ionic conductivity of the electrolyte is highly dependent on the temperature.

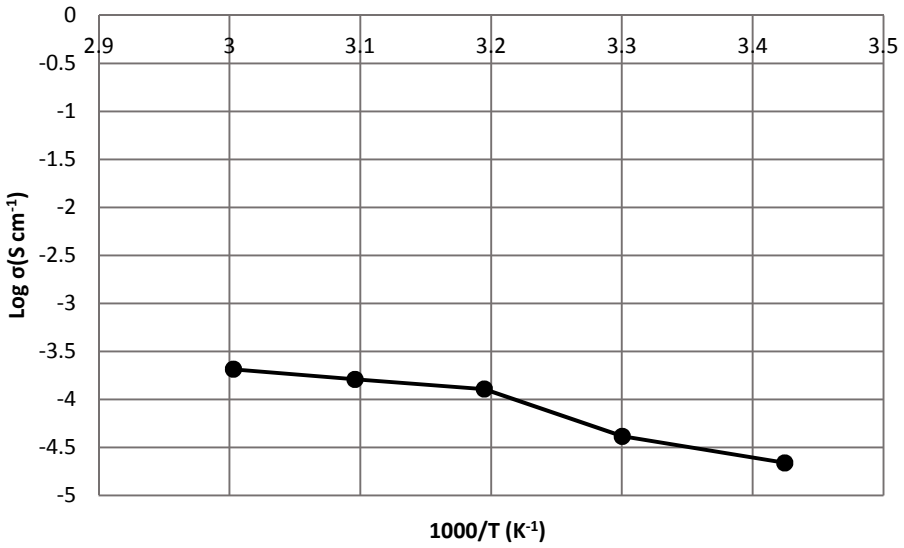

Figure 4.5 Arrhenius plot of the conductivity of polymer electrolyte PEO10LiTFSI

The Arrhenius plot of the conductivity of polymer electrolyte PEO10LiTFSI is shown in Figure 4.5. At 60˚C the conductivity of the polymer electrolyte is 7.5 X 10^{-3} S/cm.

To see the effectiveness of the glass-ceramic LATP as a suitable solid ceramic material, well known material Al_2O_3 was selected. A flexible composite solid electrolyte as shown in Figure 4.6, was fabricated with the optimum ratio of 75:25 of Al_2O_3 to organic binder.

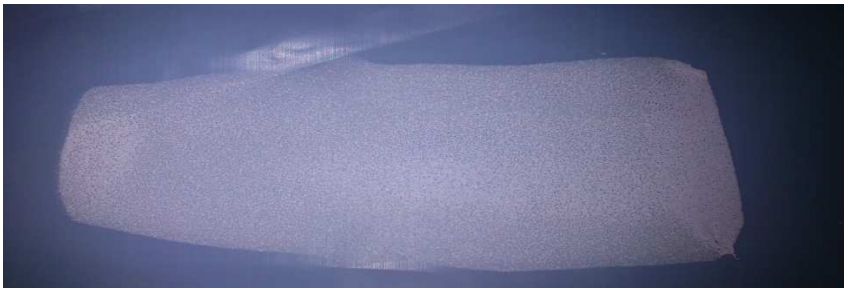

Figure 4.6 Flexible solid polymer electrolyte Al_2O_3 and organic binder in 75:25

The flexible composite electrolyte was prepared by mixing Al_2O_3 (Aldrich) with PEO10LiTFSI polymer solution in acetonitrile. The solution was casted on Teflon tape using doctor blade. After vacuum drying, the composite electrolyte was obtained. The obtained film was around 150 µm thick. The ionic conductivity of the film was studied by enclosing the film in a coin cell inside glove box. (O_2 , H_2O < 0.1 ppm)

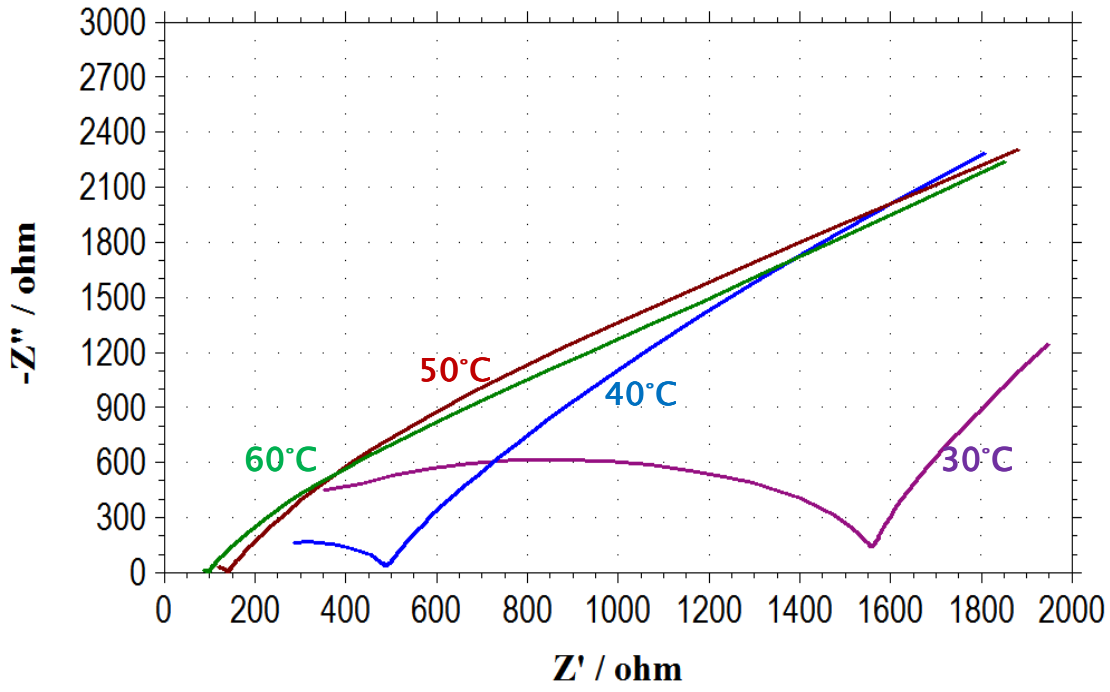

Figure 4.7 EIS solid electrolyte at 60˚C of Al_2O_3 with organic binder

Figure 4.7 shows the EIS plots of the Al_2O_3 –PEO10LiTFSI composite electrolyte. The incomplete semicircle is caused by the insufficient upper limit of 100 kHz for electrochemical workstation CHI660A. From the intercept of the inclined line, the conductivity of the composite electrolyte was studied at different temperatures as shown in Figure 4.8. EIS plots reveal that LATP is better solid ceramic material when compared to Al_2O_3.

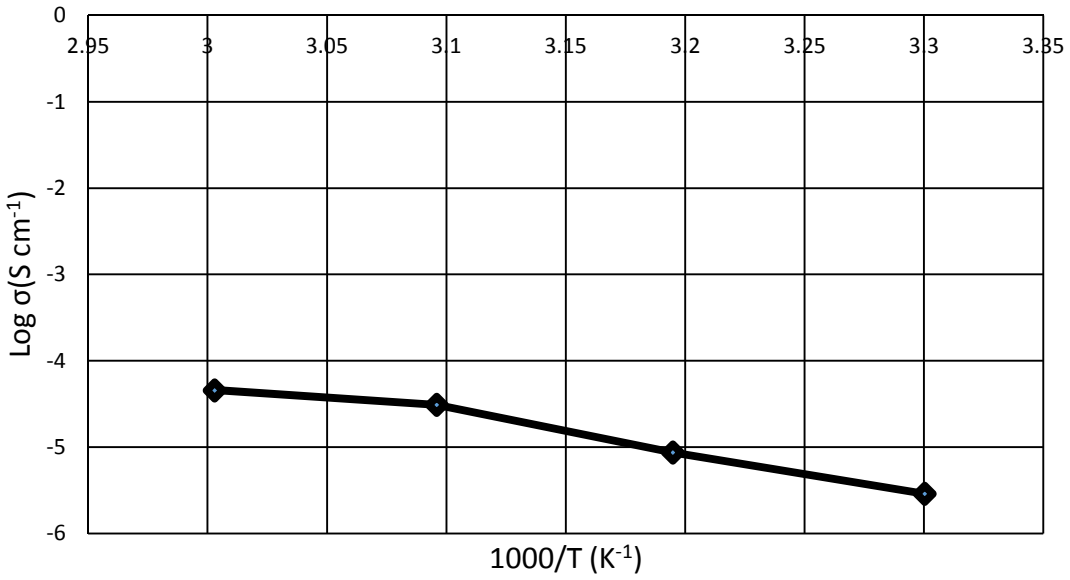

Figure 4.8 Conductivity of Composite Solid Electrolyte of Al_2O_3 and organic binder in 75:25 in relation with temperatures

The temperature dependence of the ionic conductivities of the solid electrolyte (LATP) in combination with the polymer binder PEO-10LITFSI at different compositions and temperatures was investigated. The Figure 4.9 shows the variation of the conductivity with respect to the composition ratio at various temperatures. Amongst the different ratios the optimum ratio of 75:25 is selected, since a stable and flexible film can be obtained with highest conductivity when compared to other ratios.

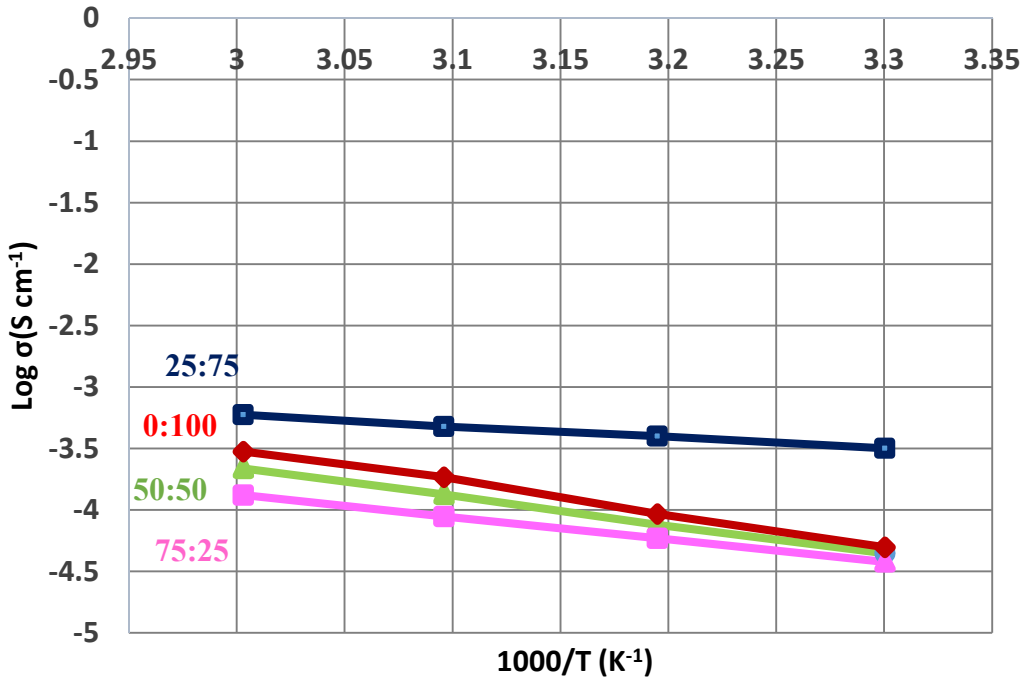

Figure 4.9 Conductivity vs Temperature of Composite Electrolyte at Different Compositions

To fabricate a practical all solid state rechargeable battery, the electrolyte must have an appreciable conductivity of the order of ~ 10^{-3} - 10^{-4} S/cm. Several researchers focused to tackle this issue. Amongst them one way was to make a thin film battery. However, fabrication of thin film batteries for large scale is cumbersome and expensive. Alternatively, pressure plays a significant role in the performance of an all solid state battery.

To investigate in this, an optimum ratio of 75:25 ratio of LATP: PEO-LITFSI was chosen, and the conductivity was measured at three different pressures. Figure 4.10 shows the variation of conductivity variation of the composite solid electrolyte with respect to temperature at the pressures of 1000 psi, 2000 psi, 3000 psi. From the experimental data it is evident that at 2000 psi the solid electrolyte has good ionic conductivity. This may be

because at 2000 psi the interfacial resistance between the solid electrolyte particles of LATP and polymer decreases, however, at much higher pressure the resistance increases.

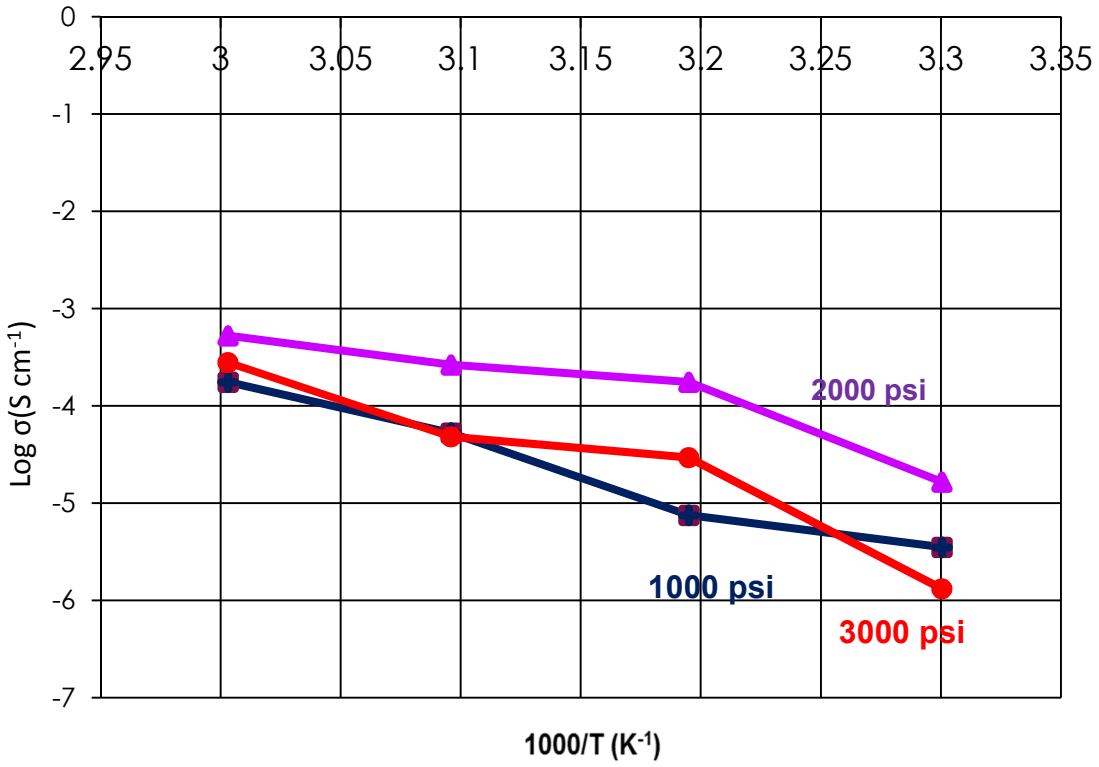

Figure 4.10 Conductivity of Composite Solid Electrolyte 75:25 in relation with pressures and temperatures

To confirm the effectiveness of PEO as an organic binder, another binder PVDF was selected and at the same ratio of 75: 25, the composite solid electrolyte was prepared. The performance of the solid electrolyte at different temperatures was studied. Figure 4.11 shows the impedance plots of the solid electrolyte of LATP with PVDF as the organic binder from the impedance plots. The conductivity of LATP-PVDF is much lower than the conductivity of LATP-PEO, which demonstrates that PEO acts as a better organic binder when compared to PVDF binder.

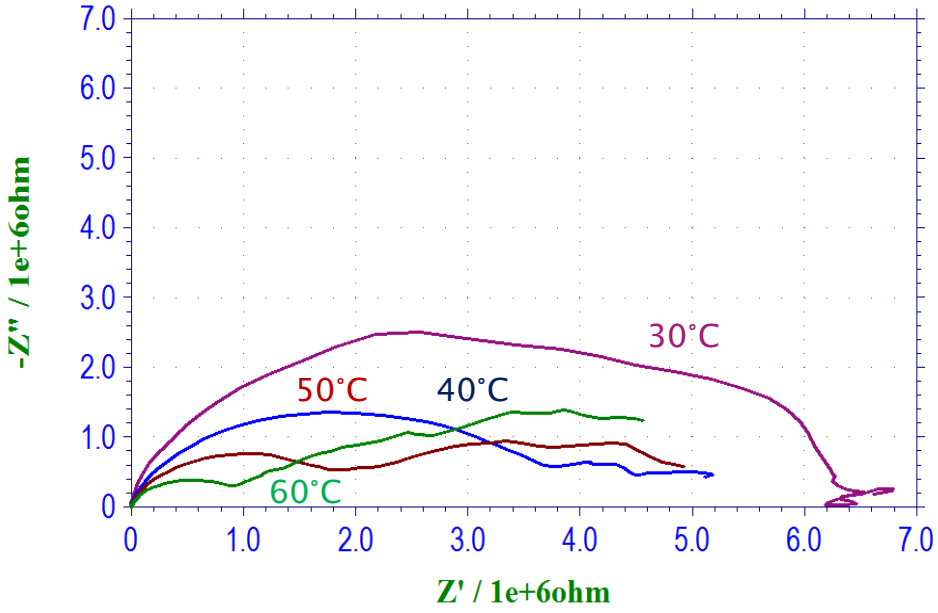

Figure 4.11 EIS plots of the solid electrolyte of LATP with PVDF as the organic binder

Figure 4.12 shows the schematic of the all solid state cell with $LiMn_2O_4$ acting as the symmetric electrodes for the composite solid electrolyte. The schematic shows that the composite solid electrolyte is sandwiched between the two asymmetric electrodes of $LiMn_2O_4$ to form an all solid state cell.

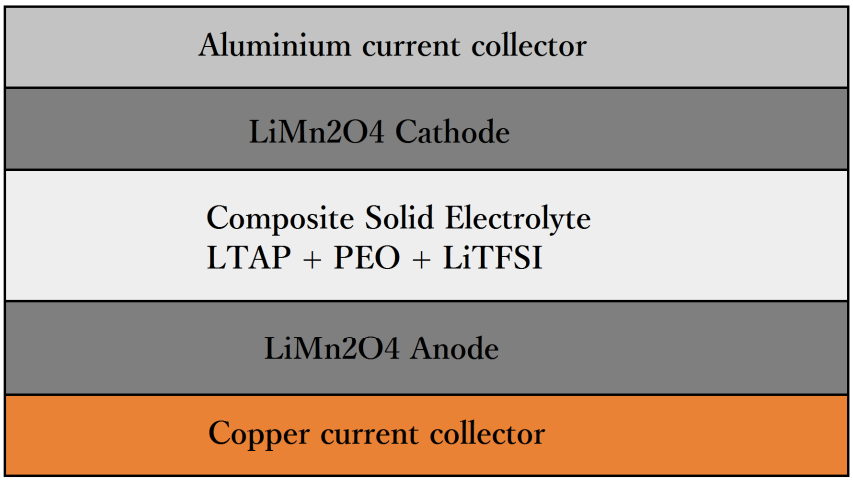

Figure 4.12 Schematic of an all solid state cell using composite solid electrolyte and symmetric electrodes

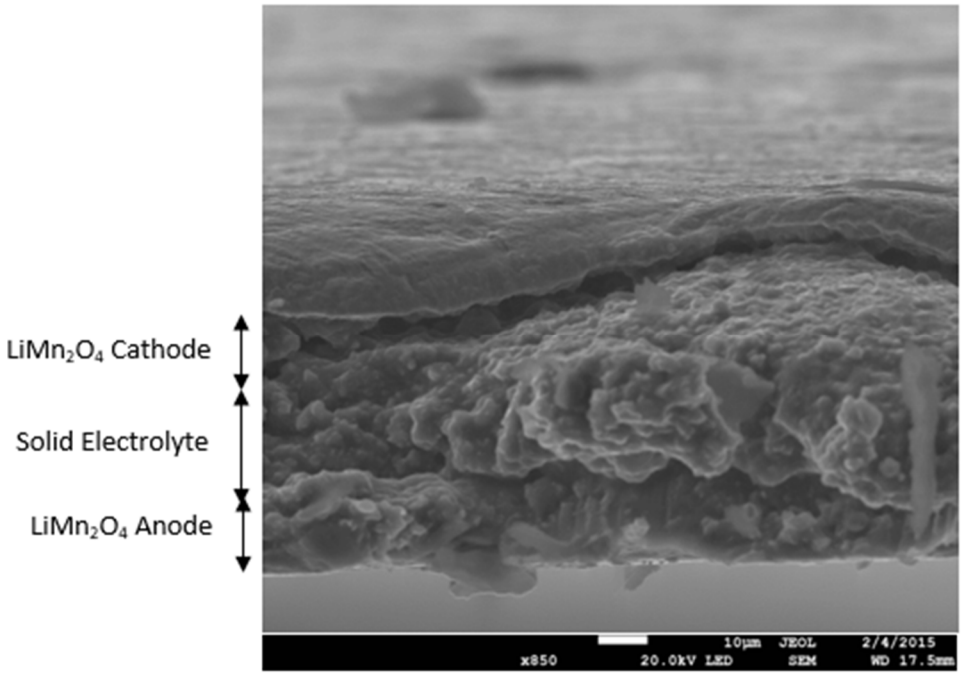

Figure 4.13 SEM of the cross-section of the Lithium Ion battery

The SEM of the cross-section of the A.S.S (Figure 4.13) lithium ion battery shows that the typical thickness of the cathode is 10 µm, while the thickness of the anode is 15 µm. From the SEM it can be seen that the composite solid electrolyte was sandwiched between the two symmetric electrodes.

Figure 4.14 shows the EIS of the A.S.S at different pressures. From the plot, it can be seen that only one semicircle was observed for each sample corresponding to each pressure. The left intercept of the semicircle with the real axis corresponds to the solid electrolyte resistance (R_{SE}) while the width of the semicircle measured along the real axis corresponds to the interfacial resistance between the electrolyte particles and electrolyte/electrode particles (R_{IR}). It can be observed that by the application of the pressure to the A.S.S cell, both the resistance's decrease indicating good contact at high pressures

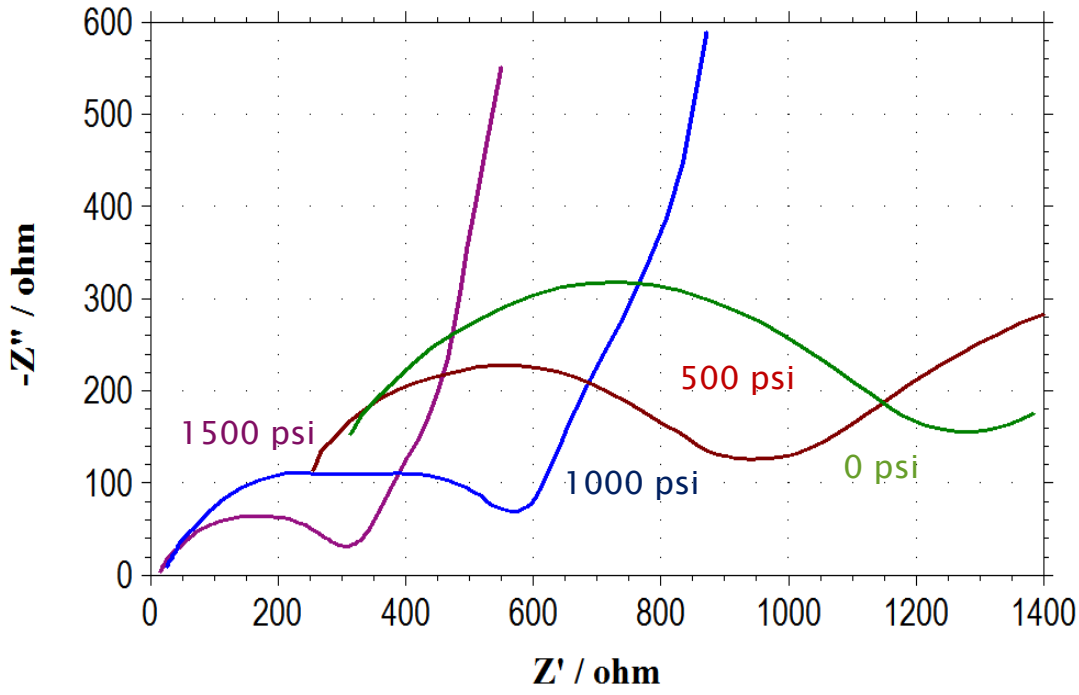

Figure 4.14 EIS plots of the A.S.S cell at different pressures

The as-fabricated all solid state battery was kept for equilibrating at 60˚C for 3 h. Later the cell was tested for 7 cycles at the operating conditions of charge cut-off of 1.7 V to a discharge cut-off of 0.25 V at 60˚C. These operating conditions were chosen according to the stability window of the solid electrolyte based on the redox potentials of $LiMn_2O_4$ [69]. Since the conduction of Li ions occurs only in the amorphous phase of PEO, cell was tested at high temperature (60˚C).

Electrochemical charge-discharge characteristics of the cell are shown in Figure 4.15. Previous research shows that solid state cells are known to struggle with electrochemical performance. It has been a challenge to get appreciable capacity and cycle life even after a few cycles [70].

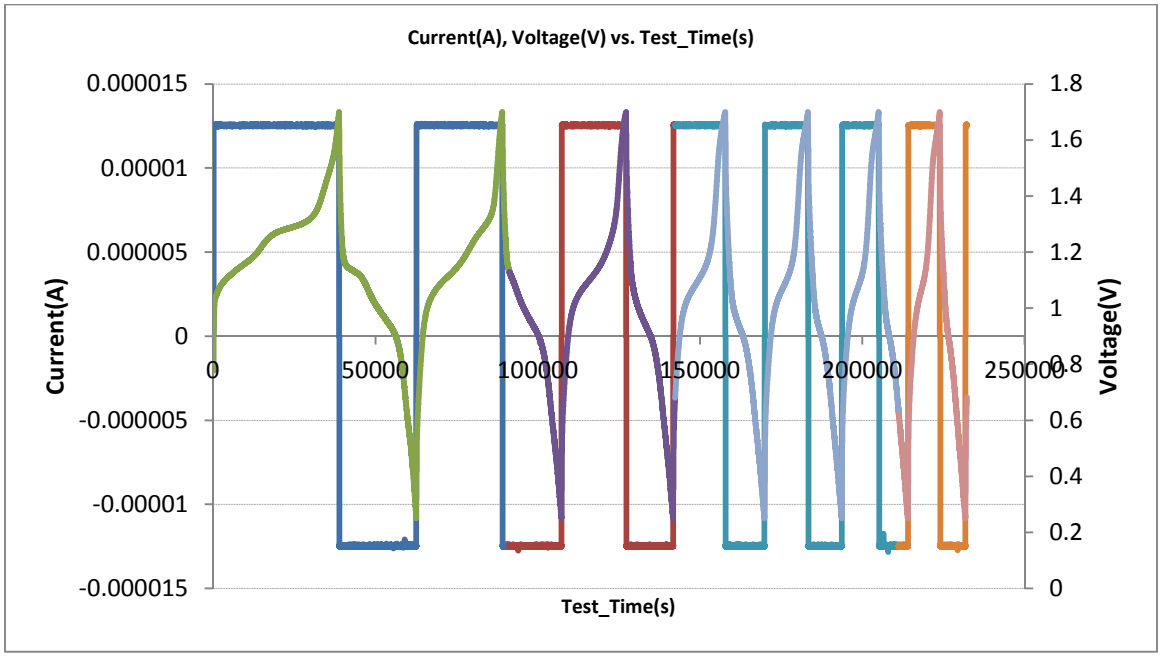

Figure 4.15 Charge-discharge characteristics of the all solid state cell $LiMn_2O_4$/S.E/$LiMn_2O_4$

Figure 4.15 shows the performance of the cell at these conditions. Although the cell with $LiMn_2O_4$ as symmetric electrodes sandwiched within LATP, has a superior capacity

in the first cycle, the capacity faded over the progress of cycles. This can be attributed to the fact that higher interface resistances are present between the components of the cell. According to the literature, there is also a considerable volume change associated with the $LiMn_2O_4$, during charge and discharge, which is approximately a 16% increase in the c/a ratio of the electrode [71]. The presence of the PEO as the organic binder in the solid electrolyte could accommodate to some volume change, but the presence of pressure during testing and fabrication of thin film battery could lead to better performance.

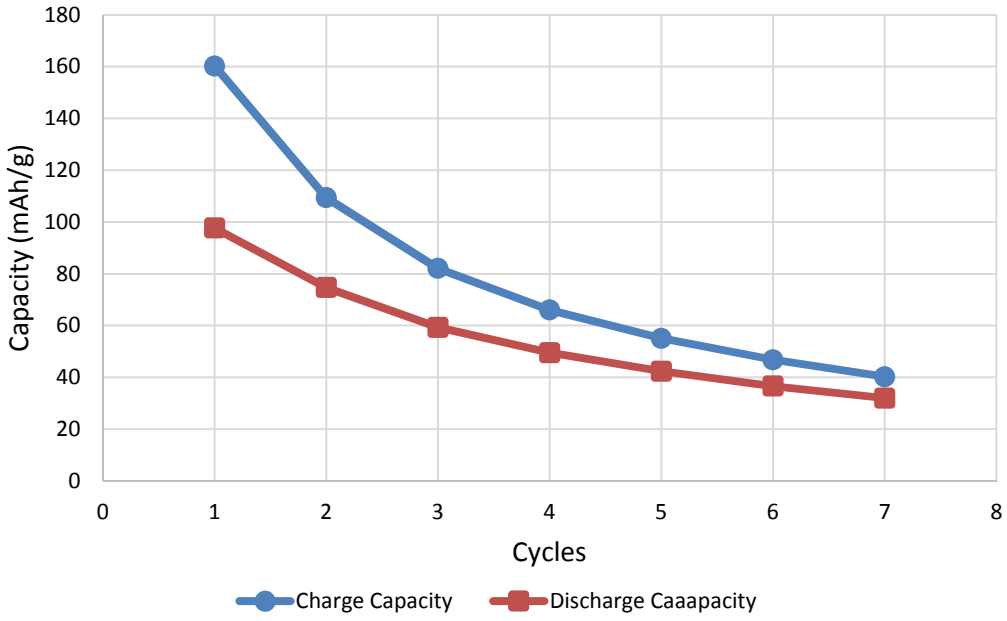

Figure 4.16 Cycle life of $LiMn_2O_4$/S.E/$LiMn_2O_4$

The same kind of solid state battery of $LiMn_2O_4$/ Solid Electrolyte/$LiMn_2O_4$ was tested at the same operating conditions but in the presence of different pressures. To achieve this, a new kind of device was utilized. Figure 4.17 shows the device wherein the stainless steel rods act as current collectors with Alumina tube aiding to hold the components together. The cell was assembled in a glove box and sealed with vacuum grease to prevent contact with atmosphere.

Figure 4.17 Schematic and picture of the device used for testing the cell under pressure

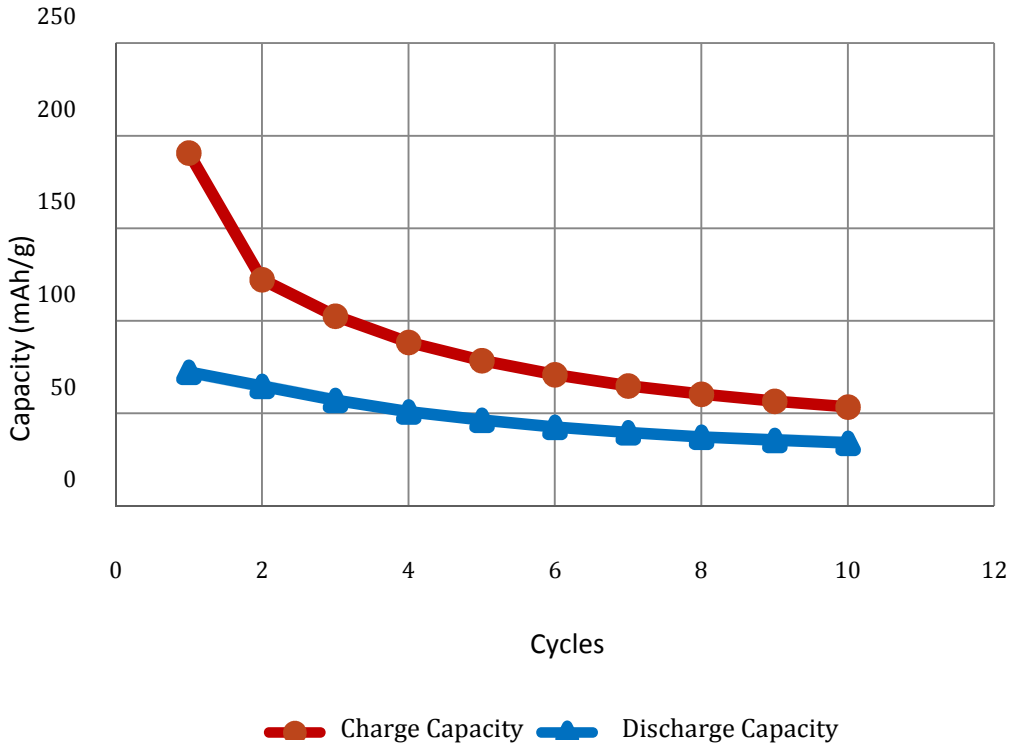

Figure 4.18 Cyclic Performance of the A.S.S. cell at 1000psi

A constant pressure of 1000 psi was applied to the battery. Figure 4.18 shows the charge/discharge characteristics of the A.S.S battery at 1000psi. From the plot it can be seen that by the application of the pressure could accommodate to the interfacial resistance between the components of the cell and also for the volume change associated with the $LiMn_2O_4$ anode. Since, $LiMn_2O_4$ anode is known to exhibit a volume change of 16% in the c/a ratio [72].

When a much higher constant pressure of 1500 psi was applied to the A.S.S cell, it can be seen from the Figure 4.19 that much better capacity retention rate could be achieved. This is mainly because of the better contact achieved amongst the components of the cell, thus reducing both the solid electrolyte resistance (R_{SE}) and interfacial resistance between the electrolyte particles and electrolyte/electrode particles (R_{IR}).

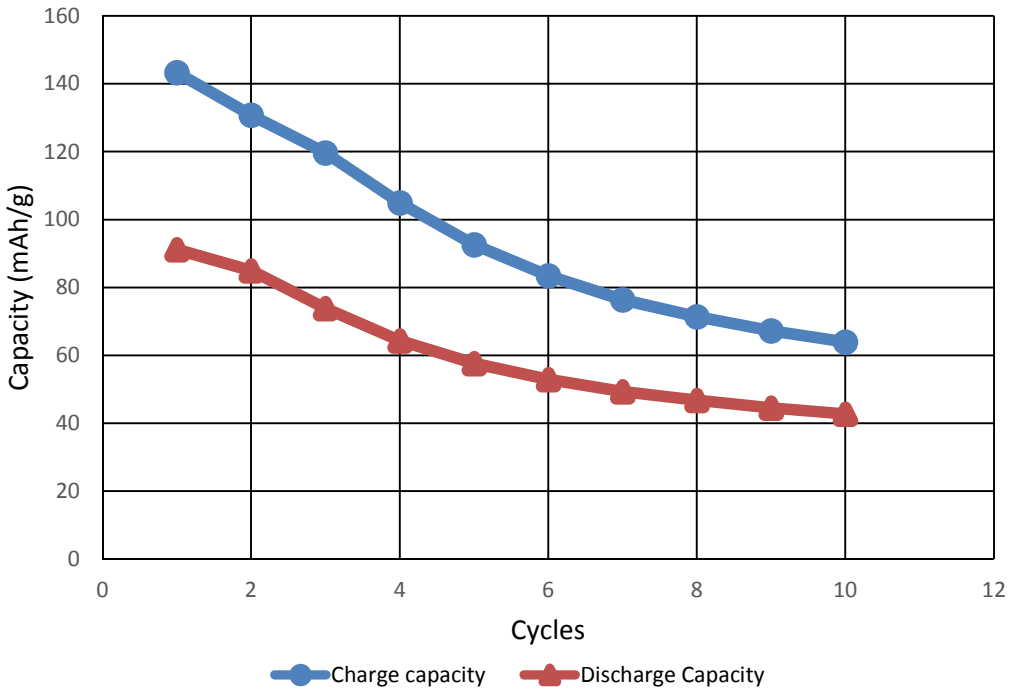

Figure 4.19 Cyclic Performance of the A.S.S. cell at 1500 psi

4.5 Summaries

An all solid state cell using $LiMn_2O_4$ as symmetric electrodes inserted between composite solid electrolytes was fabricated and tested for performance. The composite electrolyte was made with the glass-ceramic LATP in combination with an organic binder PEO with LITFSI salt. The performance of the solid electrolyte in variation of composition and temperature was analyzed. An optimum ratio of 75:25 of ceramic to binder was chosen and used as the solid electrolyte in an all solid state cell. When compared to using a pure ceramic as the solid electrolyte, addition of organic binder helped to reduce the interfacial resistance between the components of the cell. In addition, organic binder helped to accommodate partially to the volume change.

5 CONCLUSIONS AND FUTURE WORK

Lithium transition metal phosphates have gained a lot of focus in the past few years, as these materials exhibit high energy density and high voltage against Li/Li^+ Additionally, these cathode materials are less toxic and inexpensive. However, this system of cathode materials has limited applications in the commercial batteries, because of the poor electrochemical performance displayed by this system. This is mainly due to intrinsic properties such as low electronic conductivity and Mn^{+3} ion dissolution associated with Jahn-Teller distortions. This problem was addressed by adopting a modified sol-gel route to synthesis cathode particles with carbon coating thus reducing the electronic conductivity.

Additive olivines of the multi-component type of LMFP is highly favored, as this cathode material exhibits high voltage and extremely friendly. However, Mn dissolution in the electrolyte enables the material to exhibit severe capacity fade. A modified sol-gel technique and addition of 1 wt% of TMSP helped to hinder Mn dissolution in the organic liquid electrolyte. A stable cycleability was exhibited by LMFP even for 100 cycles.

A composite solid electrolyte was prepared with the glass-ceramic LATP in combination with an organic binder of PEO with LITFSI salt. At an optimum ratio of 75:25 the solid electrolyte was flexible and displayed good ionic conductivity. An all solid state cell using $LiMn_2O_4$ as symmetric electrodes inserted between composite solid electrolytes was fabricated and tested for electrochemical performance. When compared to using a pure ceramic as the solid electrolyte, addition of organic binder helped to reduce the interfacial resistance between the components of the cell. In addition, organic

binder helped to accommodate partially to the volume change. Thus, by the application of pressure greater than 1500 psi, the cell could demonstrate stable cycle performance.

LIST OF REFERENCES

LIST OF REFERENCES

[1] A. Van der Ven and G. Ceder, "Ordering in Li x (Ni 0.5 Mn 0.5) O 2 and its relation to charge capacity and electrochemical behavior in rechargeable lithium batteries," *Electrochemistry communications,* vol. 6, pp. 1045-1050, 2004.

[2] M. S. Whittingham and F. R. Gamble, "The lithium intercalates of the transition metal dichalcogenides," *Materials Research Bulletin,* vol. 10, pp. 363-371, 1975.

[3] K. Mizushima, P. Jones, P. Wiseman, and J. B. Goodenough, "Li x CoO 2 (0," *Materials Research Bulletin,* vol. 15, pp. 783-789, 1980.

[4] P. Delhaes, *Fibers and composites* vol. 2: CRC Press, 2003.

[5] Y. Jung, M. C. Suh, S. C. Shim, and J. Kwak, "Lithium insertion into disordered carbons prepared from organic polymers," *Journal of the Electrochemical Society,* vol. 145, pp. 3123-3129, 1998.

[6] S. Niu, Z. Cao, S. Li, and T. Yan, "Structure and Transport Properties of the LiPF6 Doped 1-Ethyl-2, 3-dimethyl-imidazolium Hexafluorophosphate Ionic Liquids: A Molecular Dynamics Study," *The Journal of Physical Chemistry B,* vol. 114, pp. 877-881, 2009.

[7] D. Aurbach, Y. Talyosef, B. Markovsky, E. Markevich, E. Zinigrad, L. Asraf*, et al.*, "Design of electrolyte solutions for Li and Li-ion batteries: a review," *Electrochimica Acta,* vol. 50, pp. 247-254, 2004.

[8] V. Koch, L. Dominey, C. Nanjundiah, and M. Ondrechen, "The Intrinsic Anodic Stability of Several Anions Comprising Solvent-Free Ionic Liquids," *Journal of the Electrochemical Society,* vol. 143, pp. 798-803, 1996.

[9] Y. Wang, K. Zaghib, A. Guerfi, F. F. Bazito, R. M. Torresi, and J. Dahn, "Accelerating rate calorimetry studies of the reactions between ionic liquids and charged lithium ion battery electrode materials," *Electrochimica acta,* vol. 52, pp. 6346-6352, 2007.

[10] J. W. Braithwaite, A. Gonzales, G. Nagasubramanian, S. J. Lucero, D. E. Peebles, J. A. Ohlhausen*, et al.*, "Corrosion of Lithium-Ion Battery Current Collectors," *Journal of The Electrochemical Society,* vol. 146, pp. 448-456, 1999.

[11] A. K. Padhi, K. Nanjundaswamy, and J. Goodenough, "Phospho-olivines as positive-electrode materials for rechargeable lithium batteries," *Journal of the electrochemical society,* vol. 144, pp. 1188-1194, 1997.

[12] C. Delacourt, P. Poizot, M. Morcrette, J.-M. Tarascon, and C. Masquelier, "One-step low-temperature route for the preparation of electrochemically active LiMnPO4 powders," *Chemistry of Materials,* vol. 16, pp. 93-99, 2004.

[13] T. Drezen, N.-H. Kwon, P. Bowen, I. Teerlinck, M. Isono, and I. Exnar, "Effect of particle size on LiMnPO 4 cathodes," *Journal of Power Sources,* vol. 174, pp. 949-953, 2007.

[14] J. K. Kim, J. I. Lee, and D. H. Lee, "Self-assembled block copolymers: Bulk to thin film," *Macromolecular Research,* vol. 16, pp. 267-292, 2008.

[15] L. Tan, Z. Luo, H. Liu, and Y. Yu, "Synthesis of novel high-voltage cathode material LiCoPO 4 via rheological phase method," *Journal of Alloys and Compounds,* vol. 502, pp. 407-410, 2010.

[16] N. N. Bramnik, K. Nikolowski, C. Baehtz, K. G. Bramnik, and H. Ehrenberg, "Phase transitions occurring upon lithium insertion-extraction of LiCoPO4," *Chemistry of Materials,* vol. 19, pp. 908-915, 2007.

[17] N. N. Bramnik, K. Nikolowski, D. M. Trots, and H. Ehrenberg, "Thermal stability of LiCoPO4 cathodes," *Electrochemical and Solid-State Letters,* vol. 11, pp. A89-A93, 2008.

[18] S.-Y. Chung, J. T. Bloking, and Y.-M. Chiang, "Electronically conductive phospho-olivines as lithium storage electrodes," *Nature materials,* vol. 1, pp. 123-128, 2002.

[19] A. Yamada and S.-C. Chung, "Crystal Chemistry of the Olivine-Type Li ($Mn_y Fe_{1-y}$) PO_4 and ($Mn_y Fe_{1-y}$) PO 4 as Possible 4 V Cathode Materials for Lithium Batteries," *Journal of the Electrochemical Society,* vol. 148, pp. A960-A967, 2001.

[20] T. Nakamura, Y. Miwa, M. Tabuchi, and Y. Yamada, "Structural and surface modifications of LiFePO4 olivine particles and their electrochemical properties," *Journal of the Electrochemical Society,* vol. 153, pp. A1108-A1114, 2006.

[21] A. Yamada, M. Hosoya, S.-C. Chung, Y. Kudo, K. Hinokuma, K.-Y. Liu*, et al.*, "Olivine-type cathodes: Achievements and problems," *Journal of Power Sources,* vol. 119, pp. 232-238, 2003.

[22] W. F. Howard and R. M. Spotnitz, "Theoretical evaluation of high-energy lithium metal phosphate cathode materials in Li-ion batteries," *Journal of Power Sources,* vol. 165, pp. 887-891, 2007.

[23] T. Doi, S. Yatomi, T. Kida, S. Okada, and J.-i. Yamaki, "Liquid-phase synthesis of uniformly nanosized LiMnPO4 particles and their electrochemical properties for lithium-ion batteries," *Crystal Growth & Design,* vol. 9, pp. 4990-4992, 2009.

[24] J. Yao, S. Bewlay, K. Konstantionv, V. Drozd, R. Liu, X. Wang*, et al.*, "Characterisation of olivine-type LiMn x Fe 1− x PO 4 cathode materials," *Journal of alloys and compounds,* vol. 425, pp. 362-366, 2006.

[25] P. Deniard, A. Dulac, X. Rocquefelte, V. Grigorova, O. Lebacq, A. Pasturel*, et al.*, "High potential positive materials for lithium-ion batteries: transition metal phosphates," *Journal of Physics and Chemistry of Solids,* vol. 65, pp. 229-233, 2004.

[26] D. Morgan, A. Van der Ven, and G. Ceder, "Li conductivity in Li x MPO 4 (M= Mn, Fe, Co, Ni) olivine materials," *Electrochemical and solid-state letters,* vol. 7, pp. A30-A32, 2004.

[27] X. Hou, S. Hu, W. Li, L. Zhao, Q. Ru, H. Yu*, et al.*, "Ab initio study of the effects of Ag/Mn doping on the electronic structure of LiFePO4," *Chinese Science Bulletin,* vol. 53, pp. 1763-1767, 2008.

[28] P. Tang and N. Holzwarth, "Electronic structure of FePO 4, LiFePO 4, and related materials," *Physical Review B,* vol. 68, p. 165107, 2003.

[29] S.-S. Choi, Y. S. Lee, C. W. Joo, S. G. Lee, J. K. Park, and K.-S. Han, "Electrospun PVDF nanofiber web as polymer electrolyte or separator," *Electrochimica Acta,* vol. 50, pp. 339-343, 2004.

[30] Z. Bakenov and I. Taniguchi, "Physical and electrochemical properties of LiMnPO 4/C composite cathode prepared with different conductive carbons," *Journal of Power Sources,* vol. 195, pp. 7445-7451, 2010.

[31] M. Kope, A. Yamada, G. Kobayashi, S. Nishimura, R. Kanno, A. Mauger*, et al.*, "Structural and magnetic properties of Li x (Mn y Fe 1− y) PO 4 electrode materials for Li-ion batteries," *Journal of Power Sources,* vol. 189, pp. 1154-1163, 2009.

[32] N. M. Asl, J. Keith, C. Lim, L. Zhu, and Y. Kim, "Inorganic solid/organic liquid hybrid electrolyte for use in Li-ion battery," *Electrochimica Acta,* vol. 79, pp. 8-16, 2012.

[33] K. Zaghib, M. Trudeau, A. Guerfi, J. Trottier, A. Mauger, R. Veillette*, et al.*, "New advanced cathode material: LiMnPO 4 encapsulated with LiFePO 4," *Journal of Power Sources,* vol. 204, pp. 177-181, 2012.

[34] K. Zaghib, A. Guerfi, P. Hovington, A. Vijh, M. Trudeau, A. Mauger*, et al.*, "Review and analysis of nanostructured olivine-based lithium recheargeable batteries: Status and trends," *Journal of Power Sources,* vol. 232, pp. 357-369, 2013.

[35] N. Ravet, J. Goodenough, S. Besner, M. Simoneau, P. Hovington, and M. Armand, "Abstract 127," in *196th Meeting of the Electrochem. Soc*, 1999.

[36] C. Delacourt, P. Poizot, M. Morcrette, J.-M. Tarascon, and C. Masquelier, "One-step low-temperature route for the preparation of electrochemically active LiMnPO4 powders," *Chemistry of Materials,* vol. 16, pp. 93-99, 2004.

[37] N.-H. Kwon, T. Drezen, I. Exnar, I. Teerlinck, M. Isono, and M. Graetzel, "Enhanced electrochemical performance of mesoparticulate LiMnPO4 for lithium ion batteries," *Electrochemical and Solid-State Letters,* vol. 9, pp. A277-A280, 2006.

[38] D. Wang, H. Buqa, M. Crouzet, G. Deghenghi, T. Drezen, I. Exnar*, et al.*, "High-performance, nano-structured LiMnPO 4 synthesized via a polyol method," *Journal of Power Sources,* vol. 189, pp. 624-628, 2009.

[39] J. Chen, "A review of nanostructured lithium ion battery materials via low temperature synthesis," *Recent patents on nanotechnology,* vol. 7, pp. 2-12, 2013.

[40] M. M. Thackeray, "Manganese oxides for lithium batteries," *Progress in Solid State Chemistry,* vol. 25, pp. 1-71, 1997.

[41] Y. Yoon, W. Cho, J. Lim, and D. Choi, "Solid-state thin-film supercapacitor with ruthenium oxide and solid electrolyte thin films," *Journal of power sources,* vol. 101, pp. 126-129, 2001.

[42] K. Zaghib, A. Mauger, and C. Julien, "Overview of olivines in lithium batteries for green transportation and energy storage," *Journal of Solid State Electrochemistry,* vol. 16, pp. 835-845, 2012.

[43] R. Dominko, M. Bele, M. Gaberšček, A. Meden, M. Remškar, and J. Jamnik, "Structure and electrochemical performance of Li 2 MnSiO 4 and Li 2 FeSiO 4 as potential Li-battery cathode materials," *Electrochemistry Communications,* vol. 8, pp. 217-222, 2006.

[44] Y. Kim, N. M. Asi, and J. P. Keith, "Inorganic solid/organic liquid hybrid electrolyte for li ion battery," ed: Google Patents, 2012.

[45] P. V. Wright, "Electrical conductivity in ionic complexes of poly (ethylene oxide)," *British Polymer Journal,* vol. 7, pp. 319-327, 1975.

[46] A. K. Padhi, K. Nanjundaswamy, and J. Goodenough, "Phospho-olivines as positive-electrode materials for rechargeable lithium batteries," *Journal of the electrochemical society,* vol. 144, pp. 1188-1194, 1997.

[47] S. W. Oh, S. T. Myung, S. M. Oh, K. H. Oh, K. Amine, B. Scrosati*, et al.*, "Double carbon coating of LiFePO4 as high rate electrode for rechargeable lithium batteries," *Advanced Materials,* vol. 22, pp. 4842-4845, 2010.

[48] J.-K. Kim, C.-R. Shin, J.-H. Ahn, A. Matic, and P. Jacobsson, "Highly porous LiMnPO 4 in combination with an ionic liquid-based polymer gel electrolyte for lithium batteries," *Electrochemistry Communications,* vol. 13, pp. 1105-1108, 2011.

[49] C. Delacourt, P. Poizot, M. Morcrette, J.-M. Tarascon, and C. Masquelier, "One-step low-temperature route for the preparation of electrochemically active LiMnPO4 powders," *Chemistry of Materials,* vol. 16, pp. 93-99, 2004.

[50] J. Xiao, N. A. Chernova, S. Upreti, X. Chen, Z. Li, Z. Deng*, et al.*, "Electrochemical performances of LiMnPO 4 synthesized from non-stoichiometric Li/Mn ratio," *Physical Chemistry Chemical Physics,* vol. 13, pp. 18099-18106, 2011.

[51] V. Ramar and P. Balaya, "Enhancing the electrochemical kinetics of high voltage olivine LiMnPO 4 by isovalent co-doping," *Physical Chemistry Chemical Physics,* vol. 15, pp. 17240-17249, 2013.

[52] P. Barpanda, K. Djellab, N. Recham, M. Armand, and J.-M. Tarascon, "Direct and modified ionothermal synthesis of LiMnPO4 with tunable morphology for rechargeable Li-ion batteries," *Journal of Materials Chemistry,* vol. 21, pp. 10143-10152, 2011.

[53] J.-K. Kim, C.-R. Shin, J.-H. Ahn, A. Matic, and P. Jacobsson, "Highly porous LiMnPO 4 in combination with an ionic liquid-based polymer gel electrolyte for lithium batteries," *Electrochemistry Communications,* vol. 13, pp. 1105-1108, 2011.

[54] T. Drezen, N.-H. Kwon, P. Bowen, I. Teerlinck, M. Isono, and I. Exnar, "Effect of particle size on LiMnPO 4 cathodes," *Journal of Power Sources,* vol. 174, pp. 949-953, 2007.

[55] D. Morgan, A. Van der Ven, and G. Ceder, "Li conductivity in Li x MPO 4 (M= Mn, Fe, Co, Ni) olivine materials," *Electrochemical and solid-state letters,* vol. 7, pp. A30-A32, 2004.

[56] F. Zhou, M. Cococcioni, C. A. Marianetti, D. Morgan, and G. Ceder, "First-principles prediction of redox potentials in transition-metal compounds with LDA+ U," *Physical Review B,* vol. 70, p. 235121, 2004.

[57] J. Molenda, W. Ojczyk, and J. Marzec, "Electrical conductivity and reaction with lithium of LiFe 1− y Mn y PO 4 olivine-type cathode materials," *Journal of Power sources,* vol. 174, pp. 689-694, 2007.

[58] T. Nedoseykina, M. G. Kim, S.-A. Park, H.-S. Kim, S.-B. Kim, J. Cho*, et al.*, "In situ X-ray absorption spectroscopic study for the electrochemical delithiation of a cathode LiFe 0.4 Mn 0.6 PO 4 material," *Electrochimica Acta,* vol. 55, pp. 8876-8882, 2010.

[59] C. Mi, X. Zhang, X. Zhao, and H. Li, "Synthesis and performance of LiMn 0.6 Fe 0.4 PO 4/nano-carbon webs composite cathode," *Materials Science and Engineering: B,* vol. 129, pp. 8-13, 2006.

[60] H.-J. Kim, B.-S. Jin, D.-S. Bae, S.-B. Kim, and H.-S. Kim, "Synthesis and Electrochemical Characterization of LiMn0. 6Fe0. 4PO4/C Cathode Material via a Modified-Solid State Reaction Method," *Journal of nanoscience and nanotechnology,* vol. 13, pp. 3276-3281, 2013.

[61] Y.-J. Shin, J.-K. Kim, G. Cheruvally, J.-H. Ahn, and K.-W. Kim, "Li (Mn 0.4 Fe 0.6) PO 4 cathode active material: Synthesis and electrochemical performance evaluation," *Journal of Physics and Chemistry of Solids,* vol. 69, pp. 1253-1256, 2008.

[62] D. Choi, D. Wang, I.-T. Bae, J. Xiao, Z. Nie, W. Wang*, et al.*, "LiMnPO4 nanoplate grown via solid-state reaction in molten hydrocarbon for Li-ion battery cathode," *Nano letters,* vol. 10, pp. 2799-2805, 2010.

[63] J. Duan, Y. Cao, J. Jiang, K. Du, Z. Peng, and G. Hu, "Novel efficient synthesis of nanosized carbon coated LiMnPO 4 composite for lithium ion batteries and its electrochemical performance," *Journal of Power Sources,* vol. 268, pp. 146-152, 2014.

[64] G. Appetecchi, G. Dautzenberg, and B. Scrosati, "A New Class of Advanced Polymer Electrolytes and Their Relevance in Plastic-like, Rechargeable Lithium Batteries," *Journal of The Electrochemical Society,* vol. 143, pp. 6-12, 1996.

[65] H. Aono, E. Sugimoto, Y. Sadaoka, N. Imanaka, and G. y. Adachi, "Ionic Conductivity of the Lithium Titanium Phosphate (Li1+ X M X Ti2− X (PO 4) 3, M= Al, Sc, Y, and La) Systems," *Journal of the Electrochemical Society,* vol. 136, pp. 590-591, 1989.

[66] K. Nagata and T. Nanno, "All solid battery with phosphate compounds made through sintering process," *Journal of Power Sources,* vol. 174, pp. 832-837, 2007.

[67] A. Ghosh and P. Kofinas, "PEO based block copolymer as solid state lithium battery electrolyte," *ECS Transactions,* vol. 11, pp. 131-137, 2008.

[68] W. Gorecki, M. Jeannin, E. Belorizky, C. Roux, and M. Armand, "Physical properties of solid polymer electrolyte PEO (LiTFSI) complexes," *Journal of Physics: Condensed Matter,* vol. 7, p. 6823, 1995.

[69] X. M. Wu, J. L. Liu, R. X. Li, S. Chen, and M. Y. Ma, "Preparation and characterization of LiMn2O4/Li1. 3Al0. 3Ti1. 7 (PO4) 3/LiMn2O4 thin-film battery by spray technique," *Russian Journal of Electrochemistry,* vol. 47, pp. 917-922, 2011.

[70] Y. Kim, N. M. Asi, and J. P. Keith, "Inorganic solid/organic liquid hybrid electrolyte for li ion battery," ed: Google Patents, 2012.

[71] A. Mosbah, A. Verbaere, and M. Tournoux, "Phases Li x MnO 2 λ rattachees au type spinelle," *Materials research bulletin,* vol. 18, pp. 1375-1381, 1983.

[72] B. Gee, C. R. Horne, E. J. Cairns, and J. A. Reimer, "Supertransferred Hyperfine Fields at 7Li: Variable Temperature 7Li NMR Studies of LiMn2O4-Based Spinels," *The Journal of Physical Chemistry B,* vol. 102, pp. 10142-10149, 1998.